

ANALYSIS OF UNCERTAINTY IN SIMULATED EXCHANGE OF HEAT AND
MOISTURE AT THE LAND-ATMOSPHERE INTERFACE

A
THESIS

Presented to the Faculty
of the University of Alaska Fairbanks

in Partial Fulfillment of the Requirements
for the Degree of

MASTER OF SCIENCE

By

Mihailo Jankov, B.S.

Fairbanks, Alaska

August 2005

ABSTRACT

Land surface models (LSMs) serve to describe the atmosphere-land surface exchange in numerical weather prediction models (NWPMs) and global circulation models (GCMs). The use of empirical soil and vegetation parameters in LSMs introduces uncertainty that propagates and affects predictions of the lower boundary conditions. To statistically assess that uncertainty in predicted evapotranspiration (water transport by direct evaporation from bare ground and canopy and transpiration by the canopy) and ground heat flux for natural ranges of atmospheric soil and vegetation conditions, the Gaussian Error Propagation method is utilized.

The assessed uncertainties in direct and canopy water evaporation, transpiration and ground heat flux display prominent diurnal cycles. Prediction of evapotranspiration in desert areas is limited by the uncertainty in the evaporation of water collected on the canopy and transpiration. To improve predictions of evapotranspiration the maximal canopy storage and shielding factor should be determined with higher accuracy. It is found that uncertainty in ground heat flux is particularly great in dry and warm areas covered with sandy clay loam. A better prediction of ground heat flux requires a better parameterization of thermal conductivity and a higher degree of accuracy of the pore size distribution index.

TABLE OF CONTENTS

SIGNATURE PAGE.....	i
TITLE PAGE.....	ii
ABSTRACT.....	iii
LIST OF FIGURES	vi
LIST OF TABLES.....	viii
ACKNOWLEDGEMENTS.....	ix
1. INTRODUCTION	1
REFERENCES	5
FIGURES	8
2. UNCERTAINTY OF PREDICTED EVAPOTRANSPIRATION CAUSED BY EMPIRICAL SOIL AND VEGETATION PARAMETERS	10
ABSTRACT.....	10
ZUSAMMENFASSUNG	11
2.1. INTRODUCTION	13
2.2. MODEL DESCRIPTION	15
2.2.1. MODEL SET-UP.....	15
2.2.2. SURFACE MOISTURE FLUXES	16
2.2.3. MODEL DOMAIN.....	19
2.2.4 SYNOPSIS SITUATION.....	20
2.2.5 INITIALIZATION.....	20
2.3. EXPERIMENTAL DESIGN	21

2.3.1 GAUSSIAN ERROR PROPAGATION PRINCIPLES	21
2.3.2 UNCERTAINTY ANALYSIS	22
2.3.3 ANALYSIS OF NWP RESULTS	22
2.4. RESULTS	23
2.4.1 DIRECT EVAPORATION.....	23
2.4.2 EVAPORATION OF INTERCEPTED WATER.....	25
2.4.3 TRANSPIRATION.....	27
2.5. CONCLUSIONS.....	29
ACKNOWLEDGEMENTS.....	30
REFERENCES	31
FIGURES	36
TABLES	43
3. UNCERTAINTY OF PREDICTED GROUND HEAT FLUX DENSITY.....	50
3.1 GROUND HEAT FLUX	50
3.2 ANALYSIS.....	51
3.3 RESULTS OF THEORETICAL STUDY AND NWP EXAMPLE.....	52
REFERENCES	53
FIGURES	55
4. CONCLUSIONS.....	58

LIST OF FIGURES

Figure 1.1 Resistors connected in a serial link.	8
Figure 1.2 Resistors connected in a parallel link.	9
Figure 2.1 Soil and vegetation distribution in the model domain superimposed with terrain height (upper panel) and vegetation fraction (lower panel), respectively.	36
Figure 2.2 Direct evaporation (mmh^{-1}) (solid lines) and its uncertainty (mmh^{-1}) (dashed lines) at various relative volumetric water content and potential evaporation values.	37
Figure 2.3 Temporal evolution of soil-type averaged uncertainty in direct evaporation as obtained by MM5 simulation.	37
Figure 2.4 Evaporation of intercepted water (mmh^{-1}) (solid lines) and its uncertainty (mmh^{-1}) (dashed lines) at various values of relative volumetric water content and potential evaporation for 50% vegetation fraction.	39
Figure 2.5 Horizontal distribution of uncertainty in E_{can} (mmh^{-1}) (upper panel) and accumulated precipitation (mm) (lower panel) at respective time.	40
Figure 2.6 Transpiration (mmh^{-1}) (solid lines) and its uncertainty (mmh^{-1}) (dashed lines) for various values of potential evaporation and relative volumetric water content as obtained for loam that is 50% covered with deciduous needleleaf forest.	41
Figure 2.7 Temporal evolution of statistical uncertainty in transpiration for different vegetation types as obtained from the MM5 simulation.	42

Figure 3.1 Ground heat flux density (Wm^{-2}) (solid lines) and its uncertainty (Wm^{-2}) (dashed lines) at various relative volumetric water content and soil temperature gradient values.	55
Figure 3.2 Temporal evolution of soil-type averaged uncertainty in ground heat flux density as obtained by the MM5 simulation.	56

LIST OF TABLES

Table 2.1 LSMs that use the same parameterizations as OSULSM	43
Table 2.2 Porosity (volumetric water content at saturation) and its standard deviation as used in this study.....	44
Table 2.3 Vegetation specific parameters and their standard deviations used in the study. Here, $R_{c\min}$ (sm^{-1}) and R_{gl} (Wm^{-2}) are the minimal stomatal and the maximum visible solar radiation that can be absorbed by the vegetation.	45
Table 2.4 Average relative error of direct evaporation in percent as obtained for various soil types and shielding factors.	47
Table 2.5 Average relative error in percent for all combinations of soil and vegetation-types	48
Table 3.1 Pore size distribution index (-.-) and its standard deviations as obtained from COSBY et al. (1984).....	57

ACKNOWLEDGEMENTS

This research was funded by BMBF and NSF under contracts 07ATF30 and OPP0327664, ATM0232198, respectively. I would like to thank to Dr. N. Mölders, my academic advisor and the graduate advisory committee members, Dr. G.E. Shaw, Dr. U.S. Bhatt and Dr. W.R. Simpson, for the guidance, help and support.

1. INTRODUCTION

Land surface models (LSMs) are widely used to predict the lower boundary conditions in numerical weather prediction models (NWPMs) and climate models. Typically, LSMs have three parts, the snow, soil and canopy models, and are used to predict surface fluxes of heat, moisture and matter (e.g. DOUVILLE et al., 1995; YANG et al., 1995; DESBOROUGH and PITMAN, 1998). The atmosphere-earth surface exchange cannot be resolved on the scales of NWPMs; therefore it has to be parameterized (PIELKE, 2001). These parameterizations use empirical snow, soil and vegetation parameters to describe snow, soil and vegetation characteristics.

Both parameterizations and parameter choices can affect the accuracy of LSM's predicted lower boundary conditions (e.g. SHAO and HENDERSON-SELLERS, 1996; SLATER et al., 1998). The parameters are derived from field experiments or laboratory studies. They commonly vary in nature and their variance can be on the same order of magnitude as their mean value (e.g. CLAPP AND HORNBERGER, 1978; KÖRNER et al., 1979; COSBY et al., 1984; AVISSAR, 1991). The use of parameters introduces uncertainty into the predicted quantities. This uncertainty introduced by the empirical parameters is a random error and therefore statistically assessable (MÖLDERS, 2005; MÖLDERS et al., 2005). A more elaborate discussion of different types of errors and different impacts that parameters and parameterizations have on the predictability of surface fluxes is given in the article in section 1, Chapter 2.

The random error can be statistically quantified by applying the Gaussian Error Propagation (GEP) principles (KREYSZIG, 1970; MÖLDERS, 2005; MÖLDERS et al., 2005). GEP principles will always provide the same results for the same atmospheric and soil forcing and set of parameters; therefore uncertainty can be theoretically assessed for a broad range of meteorological, snow, soil and vegetation conditions. This method is based on the derivation of each investigated quantity ϕ with respect to its dependent empirical parameters χ_i . We refer to the overall uncertainty in the quantity ϕ due to its empirical parameters as σ_ϕ (KREYSZIG, 1970)

$$\sigma_\phi = \sqrt{\sum_{i=1}^n \left(\frac{\partial \phi}{\partial \chi_i} \right)^2 (\sigma_{\chi_i})^2} \quad (1)$$

where n is the total number of dependent parameters and σ_{χ_i} is the standard deviation of the i^{th} parameter. The GEP method and the theoretical analysis are described in greater detail in the article presented in Chapter 2, in its sections 3.1 and 3.2. Therefore, here the main principles of the method are described in brief by an example from engineering, where GEP is frequently applied.

Resistances of two electric resistors have been determined several times. The resistances obtained are $R_1=150 \pm 0.9\Omega$ and $R_2=220 \pm 1.1\Omega$, where 0.9Ω and 1.1Ω are their standard deviations (σ_{R_1} and σ_{R_2}), respectively.

If the resistors are serially linked (Figure 1.1), the total resistance is given as their sum ($R=R_1+R_2$) and amounts 370Ω . To determine its standard deviation, (σ_R), GEP method is applied (see Eq. 1). Differentiation of R with respect to R_1 and R_2 yields

$$\frac{\partial R}{\partial R_1} = 1 \quad (2)$$

and

$$\frac{\partial R}{\partial R_2} = 1. \quad (3)$$

Therefore, Eq. 1 reads

$$\sigma_R = \sqrt{\left(\frac{\partial R}{\partial R_1}\right)^2 (\sigma_{R_1})^2 + \left(\frac{\partial R}{\partial R_2}\right)^2 (\sigma_{R_2})^2}. \quad (4)$$

For the respective values of σ_{R_1} , σ_{R_2} , $\frac{\partial R}{\partial R_1}$ and $\frac{\partial R}{\partial R_2}$, uncertainty in the total resistance

(σ_R) is 1.42 Ω and total resistance is represented as $R=370 \pm 1.42\Omega$.

In the case when the same resistors are coupled in a parallel link (Figure 1.2), the total resistance is

$$R = \frac{R_1 + R_2}{R_1 R_2}. \quad (5)$$

Applying the analogous procedure for this new arrangement one will obtain $R=89.19 \pm 0.36\Omega$.

This example shows how for different arrangements of R_1 and R_2 (functional dependences of R_1 and R_2) their standard deviations propagate and result in different overall standard deviations of total resistance R .

The aim of this study is to examine uncertainty caused by empirical soil and plant parameters in evapotranspiration (sum of the evaporation of soil water, water intercepted by the canopy and transpiration by plants) and ground heat flux density as used in the

Oregon State University LSM (OSULSM; CHEN and DUDHIA, 2001). Note that in accordance with common practice the flux densities are just referred to as fluxes hereafter.

To assess the meaning of the theoretical results for weather forecasting the same procedure is applied within the Penn State/National Center for Atmospheric Research (NCAR) Mesoscale Model generation 5 (e.g. MM5; DUDHIA,1993).

The results of the investigation of evapotranspiration are presented in Chapter 2 in the form of a paper. The method applied in my study is also described in this article. It is analogous for the ground heat flux density, for which it is not repeated in Chapter 3. The derivation required to determine the uncertainty in the study as well as the initial code were derived and developed by Leslie Prochaska (PROCHASKA and MÖLDERS, 2002).

The results of the uncertainty analysis in ground heat flux are presented and discussed in Chapter 3. Chapter 4 summarizes the main results and provides recommendations for future research.

REFERENCES

- AVISSAR, R., 1991: A statistical-dynamical approach to parameterize subgrid-scale land-surface heterogeneity in climate models. - *Surv. Geophys.*, **12**, 155-178.
- CHEN, F., and J. DUDHIA, 2001: Coupling an advanced land surface hydrology model with the Penn State/NCAR MM5 modeling system. Part I: Model description and implementation. - *Mon. Wea. Rev.*, **129**, 569-585.
- CLAPP, R.B., and G.M. HORNBERGER, 1978: Empirical equations for some soil hydraulic properties. - *Water Resour. Res.*, **14**, 601-604.
- COSBY, B.J., G.M. HORNBERGER, R.B. CLAPP, and T.R. GINN, 1984: A statistical exploration of the relationships of soil moisture characteristics to the physical properties of soils. - *Water Resour. Res.*, **20**, 682-690.
- DESBOROUGH, C.E. and A.J. PITMAN, 1998: The BASE land surface model, *Global and Planetary Change*, **19(1-4)**, 3-18.
- DOUVILLE, H., J.F. ROYER and J.F. MAHFOUF, 1995: A new snow parameterization for the Météo-France climate model. Part I: validation in stand-alone experiments. - *Clim. Dyn.*, **12**, 21-35.
- DUDHIA, J. 1993: A non-hydrostatic version of the Penn State-NCAR mesoscale model: validation tests and simulation of an Atlantic cyclone and cold front. - *Mon. Wea. Rev.*, **121**, 1493-1513.
- KÖRNER C., J.A. SCHEEL, and H. BAUER, 1979: Maximum leaf diffusive conductance in vascular plants. - *Photosynthetica*, **13**, 45-82.

- KREYSZIG, E., 1970: Statistische Methoden und ihre Anwendung, Vanden Hoeck & Ruprecht, Göttingen, pp. 422.
- MÖLDERS, N., 2005. Plant and soil parameter caused uncertainty of predicted surface fluxes. - Mon. Wea. Rev. (in press)
- MÖLDERS, N., M. JANKOV and G. KRAMM, 2005: Application of Gaussian error propagation principles for theoretical assessment of model uncertainty in simulated soil processes caused by thermal and hydraulic parameters. - J. Hydr. Met. (in press)
- PIELKE, R. A., 2001: Mesoscale meteorological modeling. - Academic press, San Diego, CA, 164 p.
- PROCHASKA, L. and N. MÖLDERS, 2002: Uncertainty Analysis of Quantities Predicted by OSU Land surface model. - Geophysical Institute REU report, also available at: - <http://www.gi.alaska.edu/~molders/leslie.pdf>
- SHAO, Y., and A. HENDERSON-SELLERS, 1996: Modeling soil moisture: A project for intercomparison of land surface parameterization schemes phase 2 (b). - J. Geophys. Res., **101D**, 7227-7250.
- SLATER, A. G., A.J. PITMAN and C.E. DESBOROUGH, 1998: The simulation of freeze-thaw cycles in a GCM Land Surface Scheme. - J. Geophys. Res., **103D**, 11303-11312.
- YANG, Z.L., R.E. DICKINSON, A. HENDERSON-SELLERS, AND A.J. PITMAN, 1995: Preliminary study of spin-up processes in land surface models with the first stage

data of Project for Intercomparison of Land Surface Parameterization Schemes Phase

1(a). J. Geophys. Res., **100D**, 16553-16578.

FIGURES

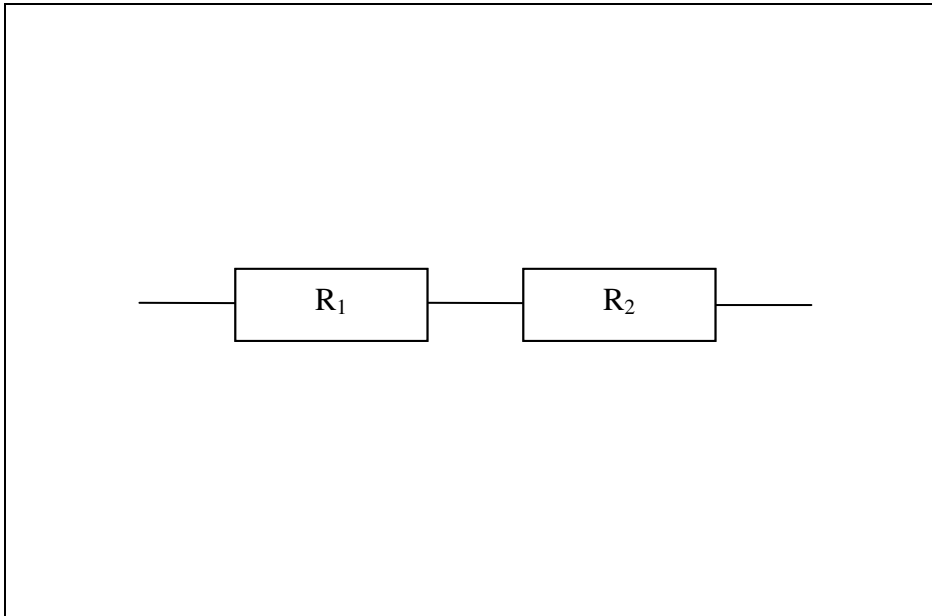


Figure 1.1 Resistors connected in a serial link.

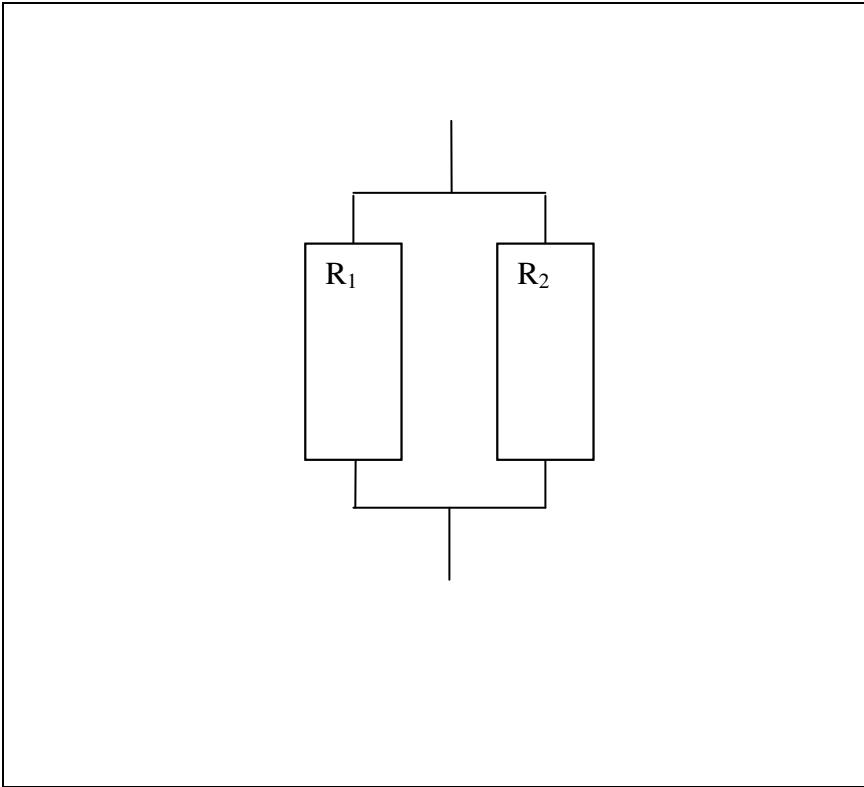


Figure 1.2 Resistors connected in a parallel link.

2. UNCERTAINTY OF PREDICTED EVAPOTRANSPIRATION CAUSED BY EMPIRICAL SOIL AND VEGETATION PARAMETERS*

ABSTRACT

All state-of-the-art numerical weather prediction models (NWPMs) have their lower boundary conditions predicted by land surface models (LSMs). Since the atmosphere-earth surface exchange of moisture is not resolvable on the scales of NWPMs, it has to be parameterized. These parameterizations use empirical parameters to describe soil and vegetation characteristics and thereby introduce uncertainty into predicted evapotranspiration, E , (sum of evaporation from the soil, E_{dir} , evaporation of the water accumulated on the canopy, E_{can} , and transpiration, E_t).

This uncertainty is assessed by applying the Gaussian Error Propagation (GEP) principles. Since GEP principles will always provide the same results for the same atmospheric and soil forcing and set of parameters, uncertainty can be theoretically assessed for a broad range of meteorological, soil and vegetation conditions. The theoretical results show that the greatest relative error is found in E_{dir} followed by E_t and E_{can} . GEP principles identified the maximal canopy storage and shielding factor as the most critical parameters in E_t and E_{can} , especially in scarcely vegetated areas, for which these parameters should be determined with higher accuracy. In well vegetated regions, uncertainty in evapotranspiration is dominated by the uncertainty in E_{dir} .

* JANKOV, M. and N. MÖLDERS, 2005: Uncertainty of Predicted Evapotranspiration Caused By Empirical Soil And Vegetation Parameters. – Met. Zeitschrift (to be submitted)

Application of the GEP analysis within the framework of a NWPM shows that uncertainty in E , E_t and E_{dir} has a distinct diurnal cycle, while that of E_{can} is strongly related to the intensity of precipitation.

ZUSAMMENFASSUNG

In modernen Wettervorhersagemodellen (NWPM) wird die untere Randbedingung mit Hilfe von Landoberflächenmodellen bestimmt. Da auf der Skala der NWPM der Austausch von Feuchte an der Grenzfläche Erde-Atmosphäre nicht aufgelöst werden kann, muss dieser parametrisiert werden. Üblicherweise verwenden solche Parametrisierungen empirische Parameter, um die Boden- und Vegetationseigenschaften zu beschreiben. Diese Parameter unterliegen einer Unsicherheit, die sich in der Evapotranspirationvorhersage (Summe aus Evaporation von Wasser vom Boden E_{dir} , Evaporation von Wasser aus dem Interzeptionsspeicher E_{can} und Transpiration E_t) fortpflanzt.

Diese Unsicherheit wird mittels Gaußscher Fehlerfortpflanzung (GEP) bestimmt. Da dieses Verfahren für ein und denselben atmosphärischen Antrieb mit denselben Bodenbedingungen und demselben Parametersatz immer dieselben Ergebnisse liefert, kann man die Unsicherheit für einen weiten Bereich möglicher meteorologischer Bedingungen sowie Boden- und Vegetationszuständen theoretisch bestimmen. Die theoretischen Ergebnisse zeigen, dass die größten relativen Fehler in der E_{dir} , gefolgt von E_{can} auftreten. Die GEP-Methode stellt den maximalen Speicherinhalt und den Abschattungsfaktor als diejenigen empirischen Parameter heraus, die am kritischsten für

die Vorhersagegenauigkeit anzusehen sind - insbesondere bei geringem Bewuchs, und deshalb mit höherer Genauigkeit gemessen werden sollten. In gut bewachsenen Gebieten beherrscht die Unsicherheit in der Evaporation vom Boden die Genauigkeit der Evapotranspirationvorhersage.

Anwendung der GEP-Verfahrens im Rahmen eines NWPM zeigt, dass die Unsicherheit der E , E_t , und E_{dir} einem Tagesgang unterliegt, während die von E_{can} von der Niederschlagsintensität abhängt.

2.1. INTRODUCTION

Contemporary numerical weather prediction (NWP) and climate models strongly rely on land surface models (LSM) to predict evapotranspiration (evaporation of soil water and water intercepted on the canopy plus transpiration) at the surface-atmosphere interface as their lower boundary condition. The accuracy of the lower boundary condition is critical for the quality of the forecasts (e.g. WEN et al., 2000; MÖLDERS, 2001). Besides errors from initial conditions and grid resolution (MÖLDERS et al., 2005; ZHANG et al., 2005) uncertainty results from the fact that the evapotranspiration is not explicitly resolvable on the spatial scale of NWP models and has to be parameterized.

The Project for Intercomparison of Land Surface Parameterizations (PILPS), for instance, showed that parameterizations can affect the accuracy of the quantities predicted by LSMs (e.g. SHAO and HENDERSON-SELLERS, 1996; SLATER et al., 1998). PILPS also showed that the parameter choice in the parameterizations can significantly affect the outcome of an LSM (e.g. SHAO and HENDERSON-SELLERS, 1996). Choosing more accurate parameters used in parameterization of stomatal resistance can reduce uncertainty in latent heat fluxes (MÖLDERS, 2005).

Imperfect parameterizations, erroneous initial conditions and heterogeneity of soil generate so-called procedural or systematic errors that exist even in the most sophisticated models (MÖLDERS, 2005). The empirical parameters used in LSMs to describe different vegetation and soil characteristics are derived from field experiments or in laboratories and their variance or standard deviation can be as great as the mean value itself (e.g., CLAPP and HORNBERGER, 1978; KÖRNER et al., 1979; COSBY et

al., 1984; AVISSAR, 1991). Commonly a mean parameter value is assigned as representative for a model's grid cell and held constant during the integration. Obviously, neglecting parameter variance can affect the ability of LSMs to describe the exchange at the atmosphere-soil interface (e.g., AVISSAR, 1991; MÖLDERS et al., 2005).

Uncertainty introduced by the use of empirical parameters is not a systematic, but rather a random error, and therefore statistically assessable (MÖLDERS et al., 2005). Due to the standard deviations of the empirical parameters any quantity (e.g. state variable, flux) calculated by help of these parameters will be burdened with a standard deviation (uncertainty). A method for statistically assessing the uncertainty in predicted quantities caused by the statistical uncertainty in empirical parameters are the Gaussian Error Propagation principles (GEP) (KREYSZIG, 1970; MÖLDERS et al., 2005). The GEP method also permits identification of critical parameters and parts of parameterizations (MÖLDERS et al., 2005). It is based on differentiation of the investigated quantities (e.g. wet canopy evaporation) with respect to its dependent parameters (e.g. shielding factor, maximal canopy storage capacity).

The aim of this study is (1) to quantify the uncertainties caused by empirical plant and soil parameters used in the equations to calculate evapotranspiration as they are typically used in state-of-the-art LSMs, and (2) to identify the parameters that cause the most uncertainty (3) and to identify critical parts of parameterizations. For ease of reading we list LSMs using these or similar parameterizations.

To generalize our results we vary the atmospheric and soil forcing over the typical ranges and calculate uncertainty in predicted evapotranspiration caused by empirical

parameters under these respective conditions. We also demonstrate the uncertainty of the predicted evapotranspiration for a four day weather forecast.

2.2. MODEL DESCRIPTION

2.2.1. MODEL SET-UP

The Penn State/National Center for Atmospheric Research (NCAR) mesoscale model generation 5 (MM5; DUDHIA, 1993) serves as the test platform for our example application. The Medium-Range Forecast (MRF) planetary boundary layer physics described by HONG and PAN (1996) is applied. Clouds on the resolvable scale are described by SCHULTZ's (1995) explicit cloud microphysical parameterization. GRELL et al.'s (1991) cumulus scheme is employed for convective clouds. Moreover DUDHIA's (1989) long-wave and shortwave radiation scheme is used.

The lower boundary conditions are calculated by Oregon State University LSM (OSULSM; CHEN and DUDHIA, 2001). LSMs using similar parameterizations of evapotranspiration are, for example, the Canadian Land Surface Scheme (CLASS) (e.g. VERSEGHY, 1991; VERSEGHY et al., 1993), the United Kingdom Meteorological Office land surface scheme (UKMO) (e.g. WARRILOW et al., 1986; GREGORY and SMITH, 1994), and the Coupled Atmosphere-Plant Soil model National Meteorological Center (CAPSNMC) (e.g. MAHRT and PAN, 1984; PAN and MAHRT, 1987; CHEN et al., 1996).

2.2.2. SURFACE MOISTURE FLUXES

Many LSMs (e.g. Simple Biosphere model, SiB, SELLERS et al., 1986; Surface Energy and Water Balance parameterization for atmospheric and hydrologic models, SEWAB; MENGELKAMP et al., 1999) like OSULSM, represent evapotranspiration, E , by the sum of direct evaporation from the soil, E_{dir} , evaporation of water intercepted by the canopy, E_{can} , and transpiration by plants through water uptake by roots, E_t (e.g. CHEN and DUDHIA, 2001),

$$E = E_{dir} + E_{can} + E_t \quad (1)$$

Direct evaporation from the ground is described by a simple linear expression (e.g. MAHFOUF and NOILHAN, 1991)

$$E_{dir} = (1 - \sigma_f) E_{pot} \frac{\eta_1 - \eta_{pwp}}{\eta_{fc} - \eta_{pwp}} \quad (2)$$

Here, E_{pot} , σ_f , η_{pwp} and η_{fc} are the potential evaporation, shielding factor (given in values from 0 to 1), wilting point and field capacity, respectively, that are determined in accordance with CHEN and DUDHIA (2001). Furthermore, η_1 is the volumetric water content in the first soil layer beneath the surface. The shielding factor indicates the fraction of a grid cell covered by green vegetation. It plays an important role for partitioning between transpiration, evaporation of intercepted water and direct evaporation from bare soil. The difference $\eta_{fc} - \eta_{pwp}$ characterizes the plant available water. Note that the soil and plant parameters are given in Tables 2.2 and 2.3, respectively.

Contribution of potential evaporation to direct evaporation, intercepted water evaporation and transpiration is calculated based on the Penman-Monteith equation. Among other LSMs the Biosphere Atmosphere Transfer Scheme (BATS, e.g., DICKINSON et al., 1993), UKMO, and CLASS use the same approach to calculate potential evaporation.

Evaporation of intercepted water is given by (e.g. CHEN and DUDHIA, 2001)

$$E_{can} = \sigma_f E_{pot} \left(\frac{W_c}{S} \right)^{0.5} \quad (3)$$

Where S ($=0.5\text{mm}$) and W_c are the maximum interceptable water that can be held on the canopy before dripping sets on and the intercepted canopy water content, respectively.

This parameterization is also used in the Interaction between Soil, Biosphere and Atmosphere model (ISBA, e.g. NOILHAN and PLANTON, 1989), SiB and UKMO, just to mention a few.

Transpiration is given by (CHEN and DUDHIA, 2001)

$$E_t = \sigma_f E_{pot} B_c \left[1 - \left(\frac{W_c}{S} \right)^{0.5} \right] \quad (4)$$

Here B_c is a non-dimensional function given as (e.g. CHEN and DUDHIA, 2001)

$$B_c = \frac{1 + \frac{\Delta}{R_r}}{1 + R_c C_h + \frac{\Delta}{R_r}} \quad (5)$$

that describes the dependence of transpiration on the canopy resistance, R_c , the surface exchange coefficient for heat and moisture, C_h , and the slope of the saturation specific

humidity curve, Δ . Furthermore, R_r is a function of air temperature, surface exchange coefficient and pressure. The canopy resistance is given by (e.g. JACQUEMIN and NOILHAN, 1990)

$$R_c = \frac{R_{c\min}}{F_1 F_2 F_3 F_4 LAI}, \quad (6)$$

where $R_{c\min}$ is the minimum stomatal resistance and LAI refers to the leaf area index. In OSULSM, LAI is set to 1. However, other models use different values of LAI for different vegetation types. The impacts of solar radiation, vapor pressure deficit, air temperature and soil moisture on stomatal resistance are considered by JARVIS-type (1976) correction functions given by

$$F_1 = \frac{\frac{R_{c\min}}{R_{c\max}} + 0.55 \frac{R_{s\downarrow}}{R_{gl}} \frac{2}{LAI}}{1 + 0.55 \frac{R_{s\downarrow}}{R_{gl}} \frac{2}{LAI}}, \quad (7)$$

$$F_2 = \frac{1}{1 + h_s [q_s(T_a) - q_a]}, \quad (8)$$

$$F_3 = 1 - b_1 (T_{ref} - T_a)^2 \quad (9)$$

and

$$F_4 = \sum_{i=1}^3 \frac{(\eta_i - \eta_{pwp}) d_{zi}}{(\eta_{fc} - \eta_{pwp})(d_{z1} + d_{z2})}, \quad (10)$$

respectively (CHEN and DUDHIA, 2001). Here R_{gl} refers to the maximum visible solar radiation that can be absorbed by the vegetation and $R_{s\downarrow}$ is the downward short-wave radiation, $R_{c\min}$ is the minimum stomatal resistance, $R_{c\max}$ ($=5000 \text{ sm}^{-1}$) is the maximum

stomatal resistance (e.g. DICKINSON et al., 1993), q_a is specific humidity and $q_s(T_a)$ is the saturated water vapor mixing ratio at given air temperature, T_a . Furthermore, h_s and b_1 ($=0.0016$) are non-dimensional empirical parameters used in the calculation of temperature and moisture stress functions. In accord with NOILHAN and PLANTON (1989), the reference temperature, T_{ref} is set to 298K. The volumetric water content of the i^{th} soil layer is denoted η_i , and d_{zi} , d_{z1} , d_{z2} represent the thickness of the i^{th} , first and second soil layer, respectively.

Other LSMs using the JARVIS-type approach are ISBA, BATS, PROGNosis of SURface Fluxes model (PROGSURF, e.g. ÁCS and HANTEL, 1998) and SiB. The Hydro-Thermodynamic Soil Vegetation Scheme (HTSVS, Kramm et al., 1996; MÖLDERS et al., 2003) uses Eqs. (8) and (10) as correction functions for the impact of soil water deficit and water vapor deficit. A correction function similar to Eq. (7) is used in SEWAB. A comprehensive overview of the models that use similar parameterizations is given in Table 2.1.

2.2.3. MODEL DOMAIN

The model domain encompasses the atmosphere over Alaska and western Canada (Figure 2.1) to a height of 100hPa. It has 23 vertical layers and 41x35 grid points in the horizontal direction with a spatial resolution of 90x90km². There are five soil layers with their bottoms at 0.1, 0.3, 0.6, 1m and 2m beneath the surface. The deepest soil layer acts as a reservoir with the gravity drainage at the bottom (CHEN and DUDHIA, 2001). One canopy layer is considered. The simulation time step is 270s.

2.2.4 SYNOPTIC SITUATION

The simulation covers August 23 1998, 1200UT through August, 27, 1998 1200UT. The synoptic situation was governed by cyclonic activity in the Bering Sea. During the first 36 hours the cyclone slowly moved north-northeastward, along the west coast of Alaska, gradually weakening. Through the middle and in the last 36 hours of the period it regenerated and moved eastward traversing the continental part of the domain. Consequently, two frontal systems on its leading edge passed over the mainland from the west coast and Aleutian Islands into the Yukon Territory. The synoptic pattern was favorable for precipitation in the western and northwestern part of Alaska at the beginning of the period. No rainfall occurred in the Yukon Territory and along the northeastern border of Alaska.

2.2.5 INITIALIZATION

The National Center for Environmental Research (NCEP) and NCAR Reanalysis Project data sets provide the initial and boundary conditions for the simulation as well as initial soil moisture and temperature. Soil type, land-cover type and terrain elevation are taken from the 1-km resolution US Department of Agriculture and 10-min resolution US Geological Survey data. The vegetation fraction assigned to each grid cell corresponds to the weighted average of the August and September monthly five-year mean green vegetation cover (0.15° resolution) data determined from advanced very high resolution radiometer measurements (GUTMAN and IGNATOV, 1998).

2.3. EXPERIMENTAL DESIGN

2.3.1 GAUSSIAN ERROR PROPAGATION PRINCIPLES

To quantify the statistical uncertainty in predicted direct evaporation $E_{\text{dir}}(\sigma_f, \eta_{\text{pwp}}, \eta_{\text{fc}})$, evaporation of intercepted water, $E_{\text{can}}(\sigma_f, S)$, and transpiration, $E_t(\sigma_f, \eta_{\text{pwp}}, \eta_{\text{fc}}, S, R_{\text{cmin}}, R_{\text{cmax}}, R_{\text{gl}}, \text{LAI}, h_s, b_1)$ we utilize GEP principles (e.g., KREYSZIG, 1970; MÖLDERS, 2005; MÖLDERS et al., 2005). This method is based on the derivation of each investigated quantity ϕ with respect to its dependent empirical parameters χ_i . We refer to the overall uncertainty in the quantity ϕ due to its empirical parameters as σ_ϕ (KREYSZIG, 1970)

$$\sigma_\phi = \sqrt{\sum_{i=1}^n \left(\frac{\partial \phi}{\partial \chi_i} \right)^2 \cdot (\sigma_{\chi_i})^2} \quad (11)$$

where n is the total number of dependent parameters and σ_{χ_i} is the standard deviation of the i^{th} parameter.

Terms $\frac{\partial \phi}{\partial \chi_i} \sigma_{\chi_i}$ are examined to describe the contribution of the i^{th} parameter to

the overall uncertainty, σ_ϕ . These contributions are denoted $\{\phi, \sigma_{\chi_i}\}$ hereafter. The

calculated relative error for the quantity ϕ is denoted as $\varepsilon_\phi = \frac{\sigma_\phi}{\phi}$. The standard

deviations for different soil and vegetation parameters are listed in Tables 2.2 and 2.3, respectively.

2.3.2 UNCERTAINTY ANALYSIS

GEP will always provide the same standard deviations for the same atmospheric and soil conditions for any given set of empirical parameters (mean values) and their corresponding standard deviations (e.g. MÖLDERS, 2005). Thus, we can calculate the uncertainty in predicted evapotranspiration for typical ranges of atmospheric and soil conditions and hence provide general results in the form of look-up tables.

Consistent with MÖLDERS (2005), we use the contribution terms, $\{\phi, \sigma_{\chi_i}\}$, to identify the most uncertain parameters. Herein, a parameter will be considered critical if its contribution term is an order of magnitude greater than those of the other parameters in the same parameterization. To identify a critical part of a parameterization we compare its contribution terms to those of other parameterizations that use the same parameters. If the same parameter causes a small overall statistical uncertainty in one parameterization versus a larger uncertainty in some other parameterization, the latter will be considered as a critical parameterization (MÖLDERS, 2005).

2.3.3 ANALYSIS OF NWP RESULTS

To demonstrate the meaning of the theoretical results we perform a simulation with MM5 for the synoptic event described above. The uncertainty in predicted evapotranspiration is calculated by the above described statistical analysis tool incorporated in MM5. The presence of the tool, of course, has no impact on the model results.

A potential correlation between the uncertainty and the spatial distribution of different soil and vegetation types, vegetation coverage, terrain elevation and simulated rainfall is investigated. To investigate the temporal evolution of uncertainty we look at the change in soil or vegetation type averaged uncertainty during the simulation period. The averaging is done by summarizing all uncertainties in evapotranspiration quantities obtained for the same soil or vegetation type and dividing by the number of grid boxes covered with the respective soil or vegetation type.

2.4. RESULTS

In the theoretical study, the natural range of meteorological variables is used. Temperature is varied from 245K to 320K and specific humidity takes values from 0.001gkg^{-1} to 15gkg^{-1} . Shortwave solar radiation and potential evaporation vary from 0Wm^{-2} to 750Wm^{-2} and from 0Wm^{-2} to 256Wm^{-2} , respectively. Volumetric water content takes values from $0.001\text{ m}^3\text{m}^{-3}$ up to porosity and canopy water varies from 0mm to 0.5mm.

2.4.1 DIRECT EVAPORATION

For all soil types statistical uncertainty increases with increasing potential evaporation and relative volumetric water content ($\frac{\eta}{\eta_s}$) for $\frac{\eta}{\eta_s} > 0.4$ (Figure 2.2), where η_s is porosity.

Below this threshold a non-linear behavior is found. This finding implies that predicted

direct evaporation is more uncertain for wet than for dry soils except for extremely dry conditions. For extremely dry soil conditions ($\frac{\eta}{\eta_s} \approx \eta_{pwp}$) uncertainty exceeds the value of the direct evaporation up to twice (relative error greater than 100%). Furthermore, uncertainty increases with increasing vegetation fraction for all soil types (Table 2.4). The greatest average relative error occurs for silty clay loam (32.87%) and the smallest one for sandy loam (6.95%) (Table 2.4). The highest absolute uncertainty is obtained for bare sandy clay loam (0.23mmh^{-1}).

On average, the individual contributions of the dependent parameters of each soil type are of the same order of magnitude (10^{-3}mmh^{-1}). Consequently none of the parameters is to be considered as critical.

In accordance with the theoretical analysis predicted direct evaporation is strongly burdened with uncertainty in stable synoptic situations that follow frontal passages in warmer part of the year. Typically, the tropical belt is more impacted due to the greater coverage by vegetation, greater insolation and higher rainfall rate. Prediction of direct evaporation is also very uncertain during summer droughts in moderately to well vegetated mid-latitude regions.

In a NWP, dry and cloud-free parts of the domain are persistently characterized with the greatest uncertainty. Wet or cloudy areas have the lowest uncertainty. There is no spatial correlation between uncertainty in E_{dir} , and the terrain elevation. The uncertainty shows a diurnal behavior as expected from the theoretical analysis. Cloud drifting and precipitation (summer thunderstorms) cause irregularities in the diurnal

pattern (e.g. Figure 2.3) for soil types with low occurrence in the same area (low sample size). In the model domain, only sandy loam, loam, clay loam and sandy clay loam soil types exist (see Figure 2.1). The greatest soil type-averaged uncertainty is found for sandy clay loam (up to 0.01mmh^{-1}) and the smallest one for sandy loam (up to 0.004mmh^{-1}) (Figure 2.3). On the domain average, the relative error in E_{dir} is 10%.

2.4.2 EVAPORATION OF INTERCEPTED WATER

Evaporation of intercepted water depends on E_{pot} , W_c , S and σ_f . Uncertainty in evaporation of water intercepted by canopy increases linearly ($r=1$) with increasing potential evaporation and canopy water content (Figure 2.4), which implies a diurnal behavior in nature. There is a strong linear dependence ($r=1$) between wet canopy evaporation and the uncertainty. The maximal uncertainty is obtained when the canopy water content and potential evaporation reach their maximum. However, the maximum achievable uncertainty differs with shielding factor. The greatest absolute values in wet canopy evaporation and its statistical uncertainty are 0.35mmh^{-1} and 0.01mmh^{-1} ($\sigma_f=1$), respectively. However, the greatest average relative error (25%) is obtained for low vegetation fraction, ($\sigma_f=0.1$). Relative error decreases exponentially as the shielding factor increases reaching a minimum of 3% at $\sigma_f=1$. These theoretical considerations imply that the uncertainty for well vegetated areas like mid-latitudes and tropics will remain close to negligible (<5%), whereas for deserts it will become more pronounced.

Uncertainty in shielding factor, $\{E_{can}, \sigma_{\sigma_f}\}$, contributes an order of magnitude more to the uncertainty in wet canopy evaporation for scarcely vegetated areas ($\sigma_f < 0.3$) than does uncertainty in maximum canopy storage, $\{E_{can}, \sigma_s\}$. For shielding factors greater than 0.4 both σ_f and S contribute equally to the uncertainty of E_{can} . Note that in the OSULSM, as it is in CLASS, maximal canopy storage for all vegetation types is represented by a single value due to a lack of data. Therefore, it is not possible to discuss uncertainty in E_{can} for different vegetation types in the NWP. Sensitivity tests, however, show that different values for S would induce only quantitative, not qualitative changes in the uncertainty of E_{can} .

Generally, theoretical analysis suggests that great uncertainty in predicted E_{can} is related to locations that are poorly covered by vegetation and exposed to a heavy rainfall. Typically coastal areas are affected by great uncertainty in prediction of E_{can} . The greatest uncertainty is expected immediately after summer thunderstorms in the mountainous terrain where the vegetation fraction tremendously decreases with height.

In the NWP, the evaporation of intercepted water and its uncertainty depend on the water and energy availability. The analysis of the NWP simulation demonstrated that the highest uncertainty is spatially related to the domain areas where precipitation occurs and the greatest uncertainty (10^{-3}mmh^{-1}) is associated with the highest precipitation rates (Figure 2.5). A diurnal course of uncertainty in evaporation of intercepted water will occur in the NWP if precipitation lasts for more than a day. It is strongly related to its dependency on the available solar energy. As expected from the theoretical study, the

spatial correlation between great uncertainty and small shielding factor is visible in NWP results. The average relative error for the NWP simulation is 5%.

2.4.3 TRANSPIRATION

Transpiration depends on potential evaporation, shielding factor, canopy water content, shortwave solar radiation, air temperature, specific humidity and plant available water. In general, the increase in all dependent variables raises transpiration and its uncertainty (e.g. Figure 2.6).

The increase in canopy water content reduces transpiration effects and as it approaches maximal canopy storage the relative error in transpiration increases exponentially (e.g. PROCHASKA and MÖLDERS, 2002). The maximum transpiration and its uncertainty amount to 0.19mmh^{-1} and 0.007mmh^{-1} for the range of conditions examined in our study.

A strong dependence of uncertainty and shielding factor is found. The relative error in transpiration exponentially decreases as shielding factor raises. The greatest relative error obtained is around 30% ($\sigma = 0.1$) and the smallest one is around 8% ($\sigma = 1$).

Typically great values of relative errors are associated with clay covered with tundra or shrubland. Small errors are found for sandy soils under cropland or grassland. The relative error slightly varies for different soil types, while its variation linked to

different vegetation characteristics is more pronounced (Table 2.5). This is due to a greater impact of the vegetation than soil parameters on the uncertainty in transpiration.

The critical parameters are maximal canopy water storage ($9.4 \cdot 10^{-4} \text{mmh}^{-1}$) followed by the shielding factor ($4.5 \cdot 10^{-4} \text{mmh}^{-1}$), the empirical parameter b_1 ($2.14 \cdot 10^{-5} \text{mmh}^{-1}$) and leaf area index ($1.8 \cdot 10^{-5} \text{mmh}^{-1}$). Contributions of the other empirical parameters used for the parameterization of transpiration are negligibly small.

The theoretical study implies that prediction of transpiration is very uncertain in warm, less vegetated areas and regions with considerable amounts of plant available water. The uncertainty is particularly pronounced after a heavy rainfall when the maximal canopy water storage is reached.

In the NWP, a moderate spatial relation between great uncertainty values and cloud-free areas is present. In the relatively drier regions, transpiration is enhanced, which results in increased uncertainty. The values obtained for wooded tundra are slightly greater than those over the other vegetation types. The uncertainty of simulated transpiration is on the order of 10^{-3}mmh^{-1} . Vegetation-type averaged uncertainty in transpiration has a distinctive diurnal cycle (Figure 2.7). The irregularity in the pattern towards the end of simulation is due to the low sample size and a thunderstorm on the back edge of a passing frontal zone. The overall average relative error for the simulation is 6%.

2.5. CONCLUSIONS

The aim of this study is to investigate uncertainty in predicted evapotranspiration caused by empirical soil and vegetation parameters. To statistically assess the uncertainty we use the Gaussian error propagation principles. Since this method provides the same standard deviations for any given set of parameters for the same atmospheric and soil forcing, we can generalize our findings by calculating uncertainty for typical ranges of atmospheric, vegetation and soil conditions. A NWPM simulation serves to illustrate the meaning of the theoretical findings for uncertainty in weather forecasting.

All investigated quantities; E_{dir} , E_{can} and E_t depend on water and energy availability and show a diurnal cycle as do their uncertainties. Uncertainty in E_{can} and E_t increases for decreasing shielding factor. The opposite is true for the uncertainty in E_{dir} . This means that over less vegetated areas uncertainty in evapotranspiration is dominated by the uncertainties in E_{can} and E_t . On the contrary, for a fully vegetated terrain uncertainty in evapotranspiration is controlled by the standard deviation in E_{dir} . In the NWP, relative error of evapotranspiration is 4.8%.

The contributions of all vegetation and soil parameters to the uncertainty in E_{dir} are of the same order of magnitude. The shielding factor contributes more to the uncertainty in E_{can} for scarcely vegetated areas ($\sigma_f < 0.3$) than does the maximum canopy storage, while their contributions even out for more vegetated regions ($\sigma_f > 0.3$). This implies that to improve the prediction of evaporation of intercepted water one must

determine the shielding factor with higher accuracy. Here, the use of actual satellite data will be an option.

The most critical parameter in E_t will be maximal canopy storage if the canopy is wet, with shielding factor following as the second most critical parameter. The contributions of all other parameters remain small. It is also found that the use of a vegetation type dependent value for maximal canopy storage is necessary. It can provide better differentiation between vegetation types and potentially increase the accuracy, not only of evaporation of intercepted water, but also transpiration, as transpiration and evaporation of intercepted water compete (cf. Eqs. (3) and (4)).

The absolute greatest relative error is obtained for E_{dir} and amounts to 32.9% (silty clay loam). The greatest relative errors in E_t and E_{can} are 29.8% ($\sigma_f = 0.1$, tundra) and 25% ($\sigma_f = 0.1$), respectively.

This study demonstrates that maximal canopy storage and shielding factor have to be determined with a higher degree of accuracy.

ACKNOWLEDGEMENTS

We thank U.S. Bhatt, G.E. Shaw, W.R. Simpson and L. Prochaska for helpful discussion and fruitful comments. This research was funded by BMBF and NSF under contracts 07ATF30 and OPP0327664, ATM 0232198, respectively.

REFERENCES

- ÁCS, F. and M. HANTEL, 1998: The land-surface flux model PROGSURF. – *Global Planet. Change*, **19**, 19-34.
- AVISSAR, R., 1991: A statistical-dynamical approach to parameterize subgrid-scale land-surface heterogeneity in climate models. - *Surv. Geophys.*, **12**, 155-178.
- BETTS, A. K. and J. H. BALL, 1994: Budget analysis of FIFE-1987 sonde data. – *J. Geophys. Res.*, **99**, 3655-3666.
- CHEN, F., K. MITCHELL, J. SCHAAKE, Y. XUE, H.L. PAN, V. KOREN, Q.Y. DUAN, M. EK., and A. BETTS, 1996: Modeling of land-surface evaporation by four schemes and comparison with FIFE observations. - *J. Geophys. Res.*, **101**, 7251-7268.
- CHEN, F., and J. DUDHIA, 2001: Coupling an advanced land surface hydrology model with the Penn State/NCAR MM5 modeling system. Part I: Model description and implementation. - *Mon. Wea. Rev.*, **129**, 569-585.
- CLAPP, R.B., and G.M. HORNBERGER, 1978: Empirical equations for some soil hydraulic properties. - *Water Resour. Res.*, **14**, 601-604.
- COSBY, B.J., G.M. HORNBERGER, R.B. CLAPP, and T.R. GINN, 1984: A statistical exploration of the relationships of soil moisture characteristics to the physical properties of soils. - *Water Resour. Res.*, **20**, 682-690.
- DICKINSON, R.E., A. HENDERSON-SELLERS, and P.J. KENNEDY, 1993: Biosphere Atmosphere Transfer Scheme (BATS) version 1e as coupled to the NCAR Community Climate Model. NCAR Technical Note, NCAR/TN-378+STR

- DUDHIA, J., 1989: Numerical study of convection observed during winter monsoon experiment using a mesoscale two-dimensional model. - *J. Atmos. Sci.*, **46**, 3077-3107.
- DUDHIA, J. 1993: A non-hydrostatic version of the Penn State-NCAR mesoscale model: validation tests and simulation of an Atlantic cyclone and cold front. - *Mon. Wea. Rev.*, **121**, 1493-1513.
- GREGORY, D. and R.N.B. SMITH, 1994: Canopy, surface and soil hydrology. - Unified Model Documentation Paper 25, 19 pp.
- GRELL, G., Y.-H. KUO, and R.J. PASCH, 1991: Semi-prognostic tests of cumulus parameterization schemes in the middle latitudes. - *Mon. Wea. Rev.*, **119**, 5-31.
- GUTMAN, G., and A. IGNATOV, 1998: The derivation of green vegetation from NOAA/AVHRR data for use in numerical weather prediction models. - *Int. J. Remote Sens.*, **19**, 1533.
- HONG, S.-Y., and H.-L. PAN, 1996: Nonlocal boundary layer vertical diffusion in a medium-range forecast model. - *Mon. Wea. Rev.*, **124**, 2322-2339.
- JACQUEMIN, B. and J. NOILHAN, 1990: Sensitivity study and validation of a land surface parameterization using the HAPEX-MOBILHY data set. - *Bound.-Layer Meteorol.*, **52**, 93-134.
- JARVIS, P.G., 1976: The interpretation of the variations in leaf water potential and stomatal conductance found in canopies in the field. - *Phil. Trans. R. Soc. London*, **B 273**, 593-610.

- KÖRNER C., J.A. SCHEEL, and H. BAUER, 1979: Maximum leaf diffusive conductance in vascular plants. – *Photosynthetica*, **13**, 45-82.
- KRAMM, G., N. BEIER, T. FOKEN, H. MÜLLER, P. SCHRÖDER, and W. SEILER, 1996: A SVAT scheme for NO, NO₂, and O₃ - model description. - *Meteorol. Atmos. Phys.*, **61**, 89-106.
- KREYSZIG, E., 1970: *Statistische Methoden und ihre Anwendung*, Vanden Hoeck & Ruprecht, Göttingen, pp. 422.
- MAHFOUF, J.-F. and J. NOILHAN, 1991: Comparative study of various formulations of evaporation from bare soil using in situ data. - *J. Appl. Meteorol.*, **9**: 351-362.
- MAHRT, L. and H. PAN, 1984: A two-layer model of soil hydrology. - *Bound.-Layer Meteorol.*, **29**, 1-20.
- MENGELKAMP, H.-T, K. WARRACH and E. RASCHKE, 1999: SEWAB – a parameterization of the Surface Energy and Water Balance for atmospheric and hydrologic models. – *Adv. Water Res.*, **23**, 165-175
- MÖLDERS, N., 2001: On the uncertainty in mesoscale modeling caused by surface parameters. - *Meteorol. Atmos. Phys.*, **76**, 119-141.
- MÖLDERS, N., U. HAFERKORN, J. DÖRING, and G. KRAMM, 2003: Long-term numerical investigations on the water budget quantities predicted by the hydro-thermodynamic soil vegetation scheme (HTSVS) – Part I: Description of the model and impact of long-wave radiation, roots, snow, and soil frost. - *Meteorol. Atmos. Phys.*, **84**, 115-135.

- MÖLDERS, N., 2005: Plant and soil parameter caused uncertainty of predicted surface fluxes. - Mon. Wea. Rev. (in press)
- MÖLDERS, N., M. JANKOV and G. KRAMM, 2005: Application of Gaussian error propagation principles for theoretical assessment of model uncertainty in simulated soil processes caused by thermal and hydraulic parameters. – J. Hydro. Meteorol. (in press)
- NOILHAN, J., and S. PLANTON, 1989: A simple parameterization of land surface processes for meteorological models. - Mon. Wea. Rev., **117**, 536-549.
- PAN, H.-L. and L. MAHRT, 1987: Interaction between soil hydrology and boundary-layer development. - Bound.-Layer Meteorol., **38**, 185-202.
- PROCHASKA, L. and N. MÖLDERS, 2002: Uncertainty Analysis of Quantities Predicted by OSU Land surface model. Geophysical Institute REU report, also available at: - <http://www.gi.alaska.edu/~molders/leslie.pdf>
- SCHULTZ, P., 1995: On explicit cloud physics parameterization for operational numerical weather prediction. - Mon. Wea. Rev., **123**, 3321-3343.
- SELLERS, P.J., Y. MINTZ, Y. C. SUD AND A. DALCHER, 1986: A simple biosphere model (SiB) for use within general circulation models. – J. Atmos. Sci., **43**,: 505-531.
- SHAO, Y., and A. HENDERSON-SELLERS, 1996: Modeling soil moisture: A project for intercomparison of land surface parameterization schemes phase 2 (b). - J. Geophys. Res., **101D**, 7227-7250.

- SLATER, A. G., A.J. PITMAN and C.E. DESBOROUGH, 1998: The simulation of freeze-thaw cycles in a GCM Land Surface Scheme. - *J. Geophys. Res.*, **103D**, 11303-11312.
- VERSEGHY, D.L., 1991: CLASS – A Canadian land surface scheme for GCMs, 1, soil model. - *Int. J. Climatol.*, **11**, 111-133.
- VERSEGHY, D.L., N.A. McFARLANE, and M. LAZARE, 1993: A Canadian Land Surface Scheme for GCMs:II. Vegetation model and coupled runs. - *Int. J. Climatol.*, **13**, 347-370.
- WARRILOW, D.A., A.B. SANGSTER and A. SLINGO, 1986: Modelling of land surface processes and their influence on the European climate. - Technical report, no. DCTN38, UK Meteorological Office, Bracknell, Berks.
- WEN, L., Y. WEI, C. A. LIN, M. BELAND, R. BENOIT and Y. DELAGE, 2000: The Role of Land Surface Schemes in Short-Range, High Spatial Resolution Forecasts. - *Mon. Wea. Rev.*, **128**, 3605–3617.
- ZHANG, M.H., W. Y. LIN, S. A. KLEIN, J. T. BACHMEISTER, S. BONY, R.T. CEDERWALL, A. D. DEL GENIO, J. J. HACK, N. G. LOEB, U. LOHMANN, P. MINNIS, I. MUSAT, R. PINCUS, P. STIER, M. J. SUAREZ, M. J. WEBB, J. B. WU, S. C. XIE, M. –S. YAO and J. H. ZHANG, 2005: Comparing clouds and their seasonal variations in 10 atmospheric general circulation models with satellite measurements. – *J. Geophys. Res.*, **110**, D15S02, doi: 10.1029/2004JD005021.

FIGURES

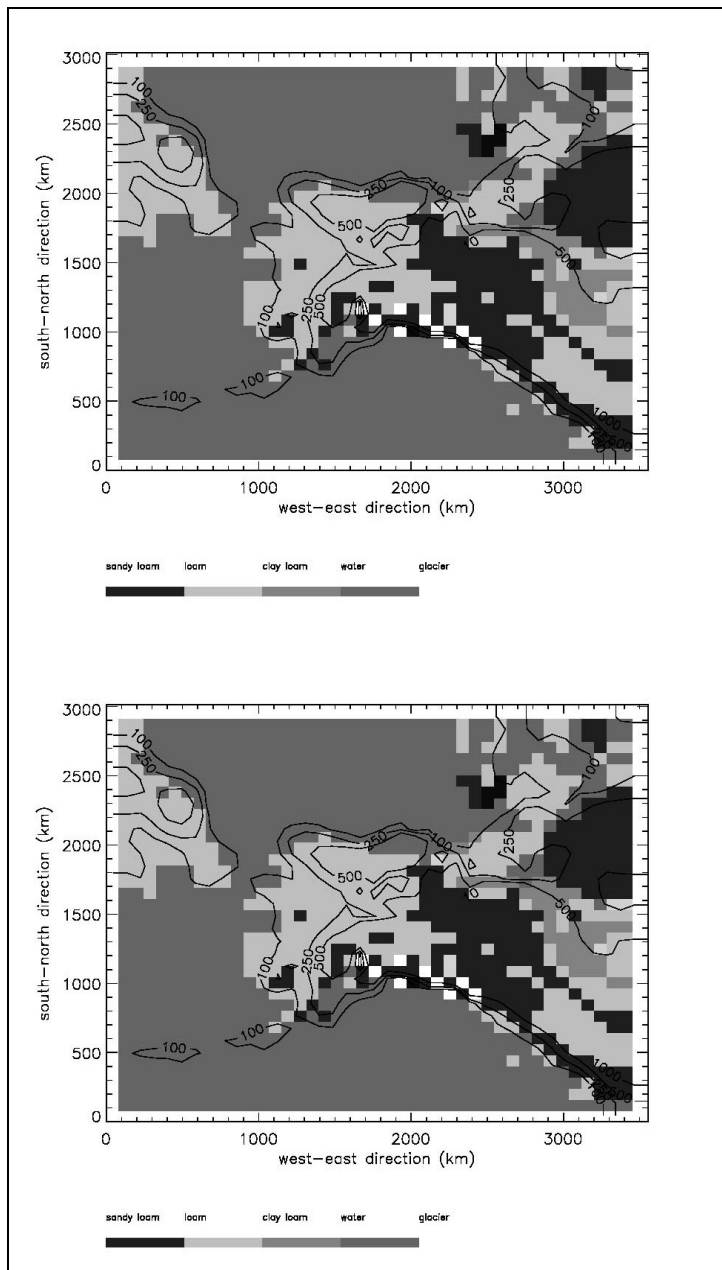


Figure 2.1 Soil and vegetation distribution in the model domain superimposed with terrain height (upper panel) and vegetation fraction (lower panel), respectively.

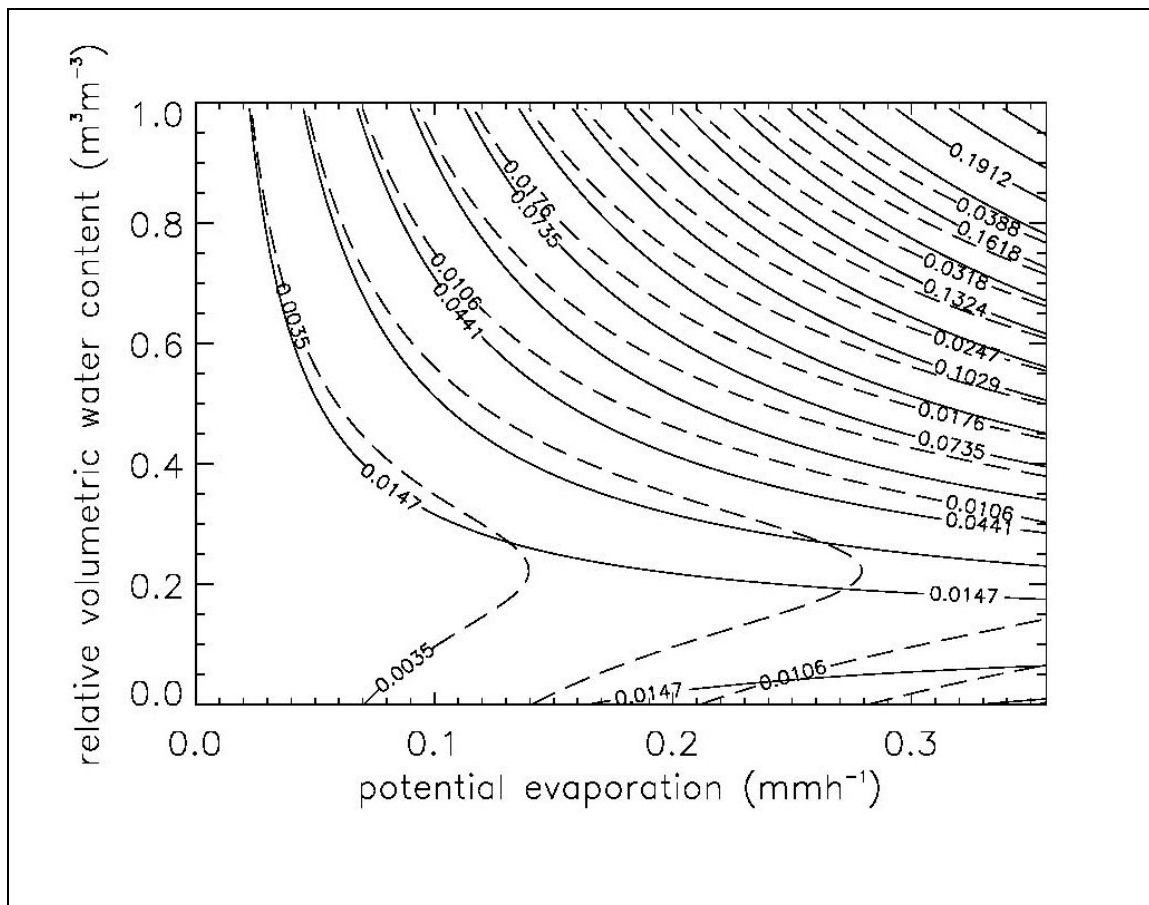


Figure 2.2 Direct evaporation (mmh^{-1}) (solid lines) and its uncertainty (mmh^{-1}) (dashed lines) at various relative volumetric water content and potential evaporation values. Example shown is for silty clay loam with 80% vegetation fraction. Plots for all other soil types combined with other vegetation fractions show the same qualitative behavior.

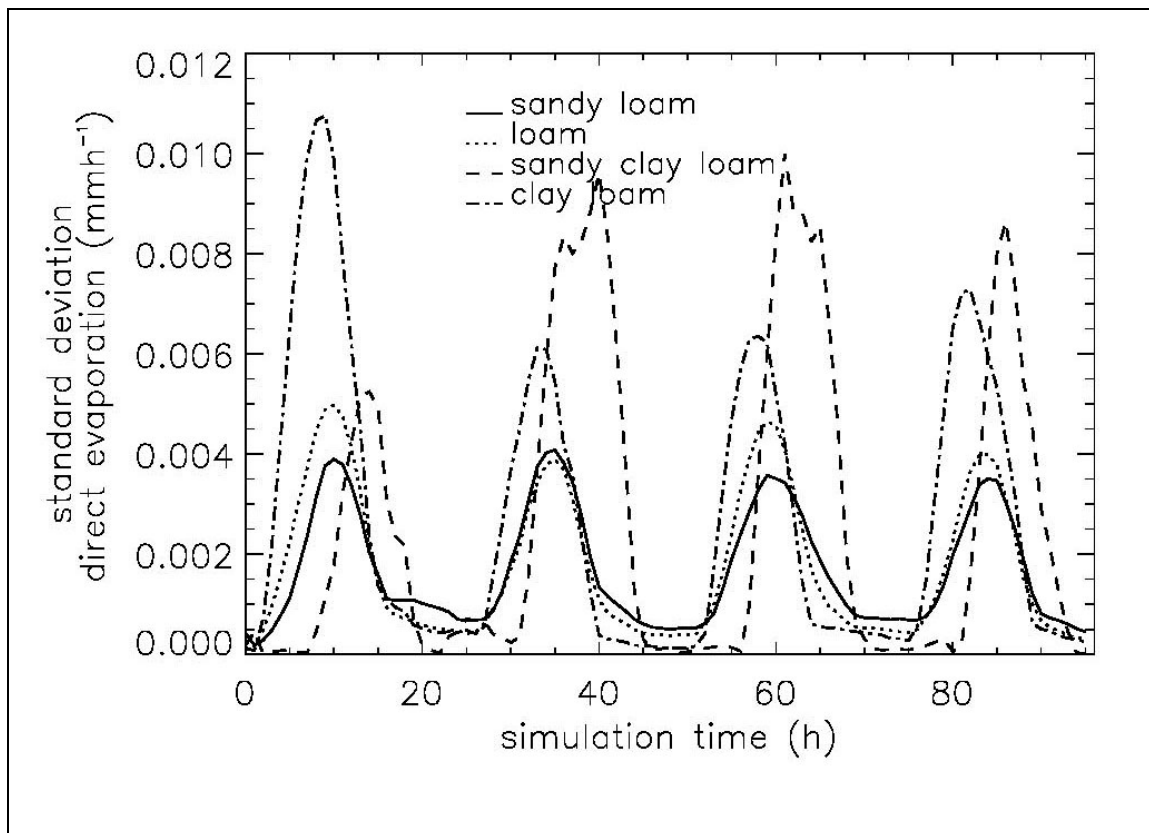


Figure 2.3 Temporal evolution of soil-type averaged uncertainty in direct evaporation as obtained by MM5 simulation. The shift in maxima is related to the location where the soil types occur most often in the domain. More western locations have their maxima later than the more eastern ones.

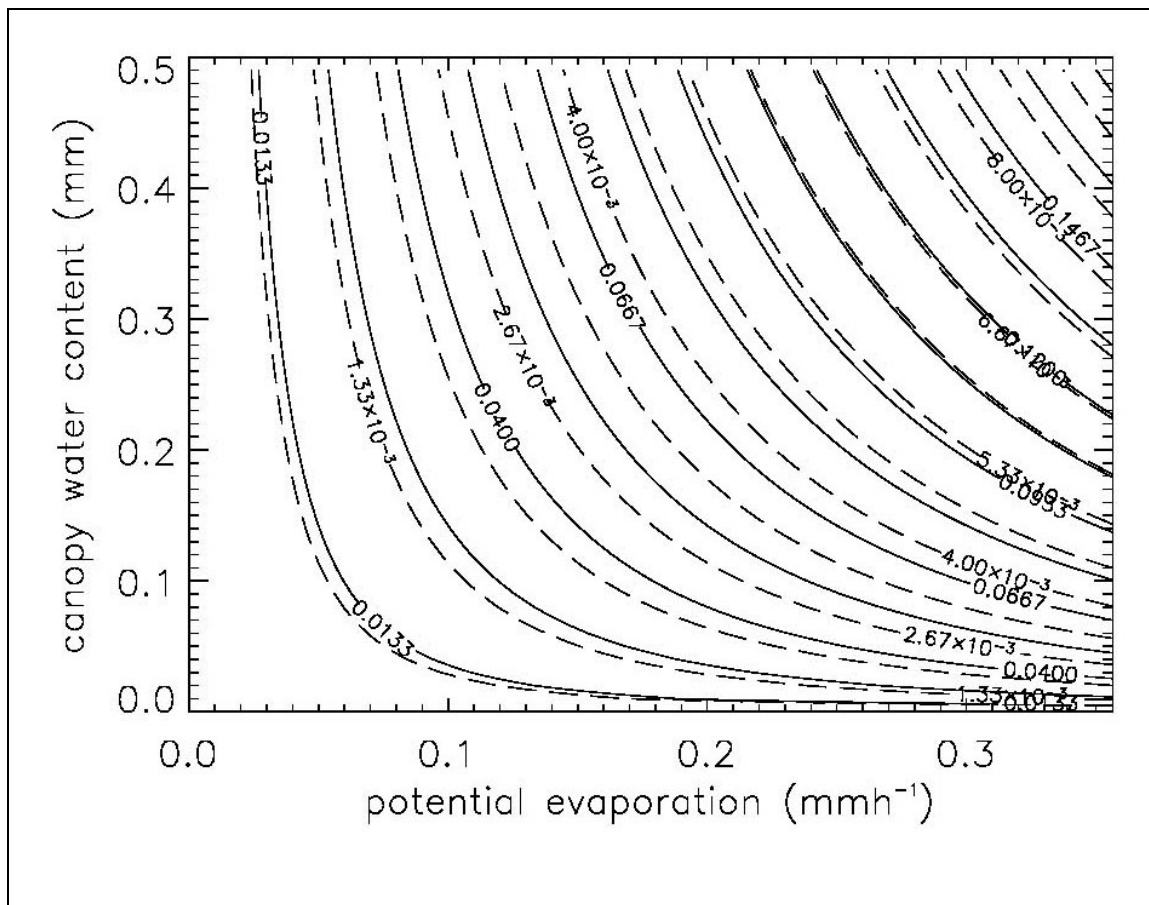


Figure 2.4 Evaporation of intercepted water (mmh^{-1}) (solid lines) and its uncertainty (mmh^{-1}) (dashed lines) at various relative volumetric water content and potential evaporation for 50% vegetation fraction. Plots for other vegetation fractions show the same behavior. Note that sensitivity studies show that different maximal storage capacity, as it should occur for different vegetation types, shows a similar qualitative behavior.

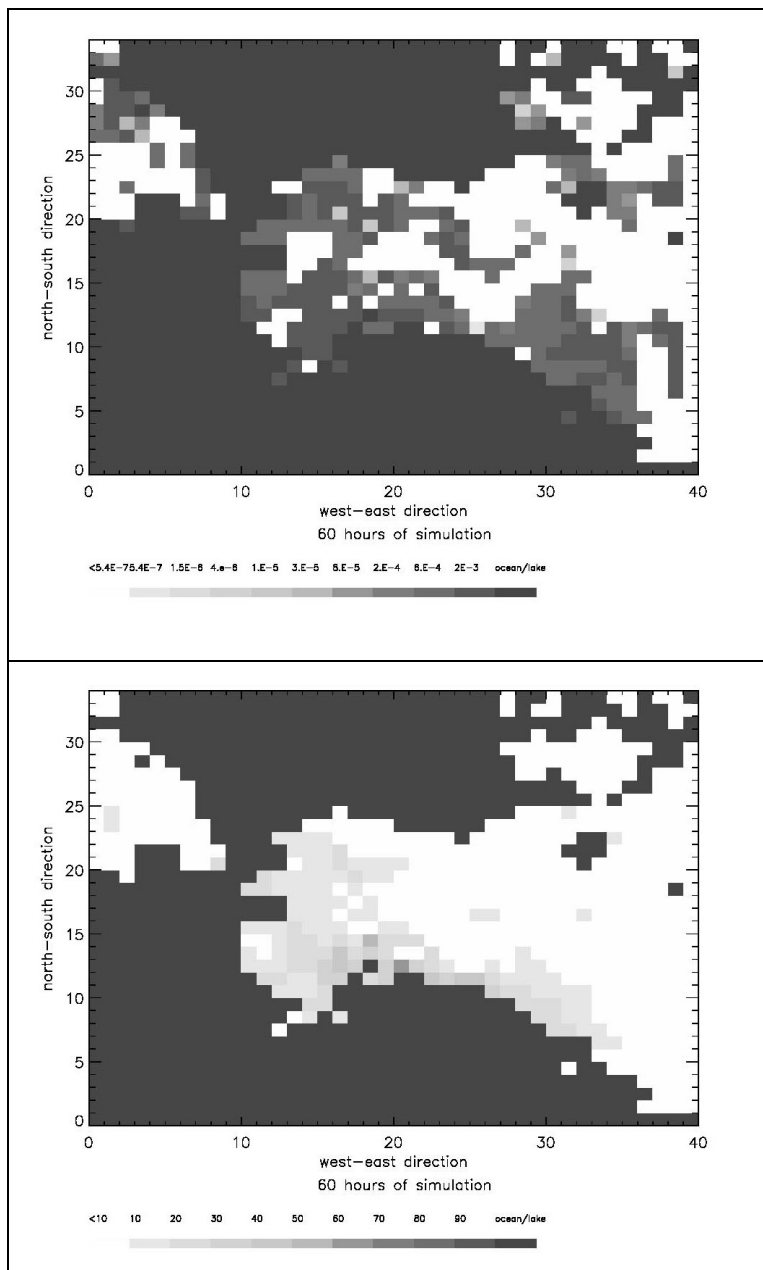


Figure 2.5 Horizontal distribution of uncertainty in E_{can} (mmh^{-1}) (upper panel) and accumulated precipitation (mm) (lower panel). The spatial correlation between uncertainty in E_{can} and precipitation is present for the entire period of the model simulation.

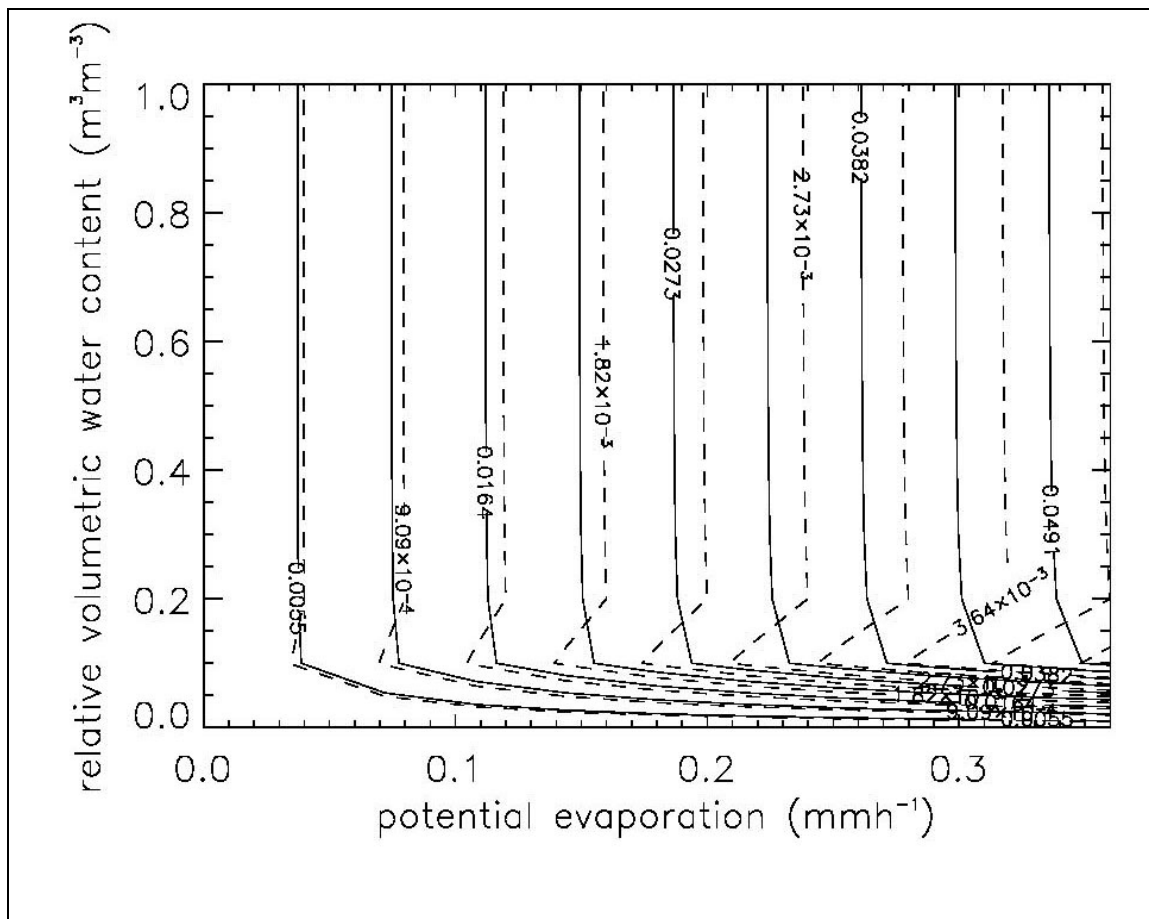


Figure 2.6 Transpiration (mmh^{-1}) (solid lines) and its uncertainty (mmh^{-1}) (dashed lines) for various values of potential evaporation and relative volumetric water content as obtained for loam that is 50% covered with deciduous needleleaf forest. Plots displaying dependency of evapotranspiration and its statistical uncertainty for all other combinations of potential evaporation, temperature, specific humidity and solar radiation show a similar qualitative behavior.

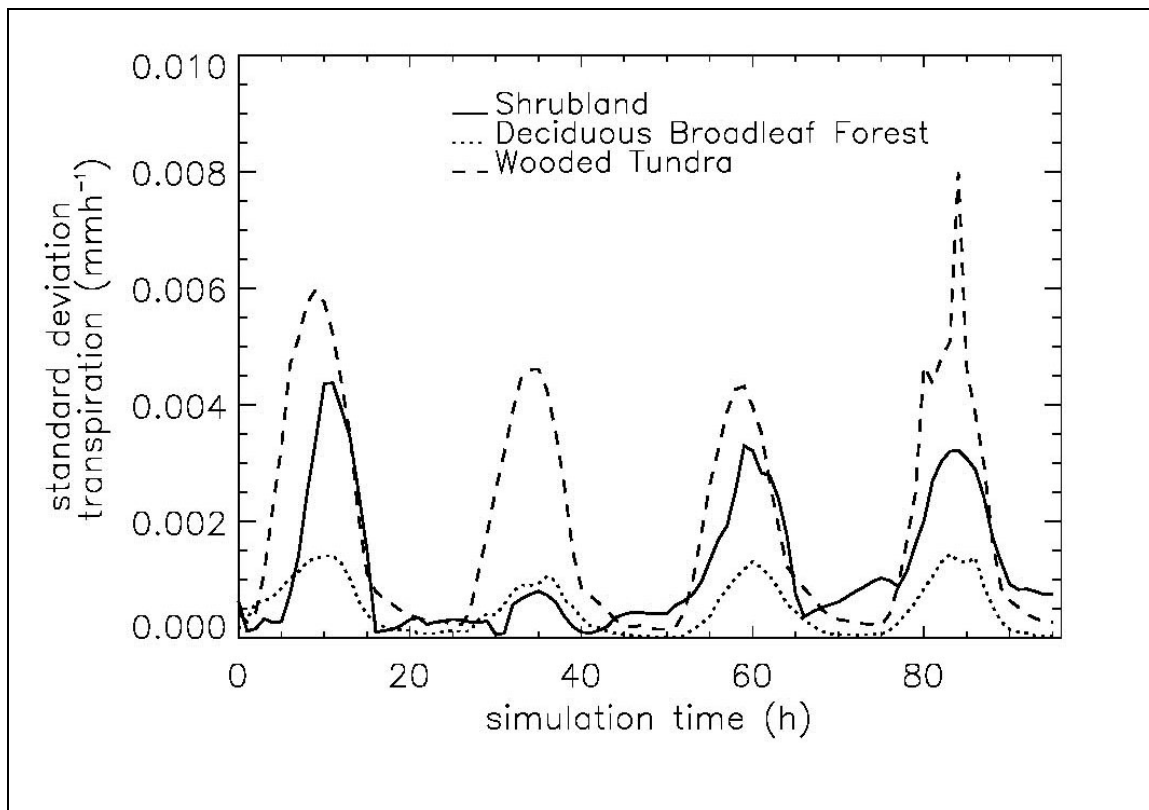


Figure 2.7 Temporal evolution of statistical uncertainty in transpiration for different vegetation types as obtained from the MM5 simulation. Note that other vegetation types occurring in the model domain also show a diurnal cycle.

TABLES

Table 2.1 LSMs that use the same parameterizations as OSULSM.

LSM	Parameterizations			
	E_{dir}	E_{can}	E_t	E_{pot}
BATS	-	-	+	+
CLASS	-	-	-	+
HTSVS	-	-	+	-
ISBA	+	+	+	-
PROGSURF	+	-	-	-
SEWAB	-	-	+	-
SIB	-	+	+	-
UKMO	-	+	-	+

Table 2.2 Porosity (volumetric water content at saturation) and its standard deviation as used in this study. Parameters and standard deviations are taken from COSBY et al. (1984). Note that the same standard deviations are assumed for field capacity and wilting point.

Soil type	$\eta_s \pm \sigma_{\eta_s}$ (m^3m^{-3})
Sand	0.339 ± 0.014
Loamy Sand	0.421 ± 0.020
Sandy Loam	0.434 ± 0.014
Silty Loam	0.476 ± 0.017
Silt	0.476 ± 0.017
Loam	0.439 ± 0.017
Sandy Clay Loam	0.404 ± 0.034
Silty Clay Loam	0.464 ± 0.043
Clay Loam	0.465 ± 0.037
Sandy Clay	0.406 ± 0.015
Silty Clay	0.468 ± 0.043
Light Clay	0.468 ± 0.039

Table 2.3 Vegetation specific parameters and their standard deviations used in the study. Here, $R_{c\min}$ (sm^{-1}) and R_{gl} (Wm^{-2}) are the minimal stomatal and the maximum visible solar radiation that can be absorbed by the vegetation. The empirical parameter h_s is used in Eq. (8). The value for maximal canopy resistance $R_{c\max}$ is equal to 5000 sm^{-1} for all vegetation types with a standard deviation of 500 sm^{-1} . Standard deviations for R_{gl} and h_s are estimated as 5% of the value. Standard deviation of $R_{c\min}$ is about 10% and in broad agreement with the results from BETTS and BALL (1994).

	Cropland/ Pasture	Irrigated Cropland/ Pasture	Non- irrigated/ cropland and pasture	Cropland/ Grassland	Cropland/ Woodland	Grassland	Shrubla nd	Shrubland/ Grassland	Savanna	Deciduous Broadleaf
$R_{c\min} \pm \sigma_{R_{c\min}}$	40 ± 4	40 ± 4	40 ± 4	40 ± 4	70 ± 7	40 ± 4	300 ± 30	170 ± 17	70 ± 7	100 ± 10
$R_{gl} \pm \sigma_{R_{gl}}$	100 ± 5	100 ± 5	100 ± 5	100 ± 5	65 ± 3.2	100 ± 5	100 ± 5	100 ± 5	65 ± 3.2	30 ± 1.5
$h_s \pm \sigma_{h_s}$	36.25 ± 1.8	36.25 ± 1.8	36.25 ± 1.8	36.25 ± 1.8	44.14 ± 2.2	36.35 ± 1.8	42 ± 2.1	39.18 ± 1.9	54.53 ± 2.7	54.53 ± 2.7

Table 2.3 continued

	Deciduous Needleleaf	Evergreen Broadleaf	Evergreen needleleaf	Mixed Forest	Herb. Wetland	Wooded Wetland	Herb. Tundra	Wooded Tundra	Mixed Tundra	Tundra
$R_{c\min} \pm \sigma$	150 ± 15	150 ± 15	125 ± 12.5	125 ± 12.5	40 ± 4	100 ± 10	150 ± 15	150 ± 15	150 ± 15	200 ± 15
$R_{gl} \pm \sigma_{R_{gl}}$	30 ± 1.5	30 ± 1.5	30 ± 1.5	30 ± 1.5	100 ± 5	30 ± 1.5	100 ± 5	100 ± 5	100 ± 5	100 ± 5
$h_s \pm \sigma_{h_s}$	47.35 ± 2.3	41.69 ± 2.1	47.35 ± 2.3	51.93 ± 2.6	60 ± 3	51.93 ± 2.6	42 ± 2.1	42 ± 2.1	42 ± 2.1	42 ± 2.1

Table 2.4 Average relative error of direct evaporation in percent as obtained for various soil types and shielding factors. Note that direct evaporation and its uncertainty for fully covered ground is equal to 0 mmh^{-1} [see Eq. (2)], therefore not shown.

	Shielding factor									
	0	0.1	0.2	0.3	0.4	0.5	0.6	0.7	0.8	0.9
Sand	7.96	8.05	8.18	8.37	8.64	9.08	9.84	11.30	14.68	26.20
Loamy sand	9.95	10.05	10.21	10.23	10.44	10.81	11.46	12.75	15.85	26.90
Sandy loam	6.95	7.06	7.21	7.42	7.74	8.24	9.08	10.66	14.21	25.98
Silty loam	8.09	8.19	8.32	8.51	8.80	9.24	10.01	11.48	14.88	26.40
Silt	8.09	8.19	8.32	8.51	8.80	9.24	10.01	11.48	14.88	26.40
Loam	8.38	8.48	8.60	8.78	9.05	9.49	10.23	11.67	15.01	26.20
Sandy clay loam	17.23	17.27	17.33	17.43	17.56	17.79	18.20	19.06	21.30	30.59
Silty clay. loam	20.64	20.65	20.73	20.81	20.93	21.12	21.48	22.23	24.24	32.87
Clay loam	16.90	16.94	17.02	17.11	17.25	17.49	17.92	18.80	21.12	30.57
Sandy clay	8.34	8.43	8.56	8.74	9.01	9.45	10.19	11.64	14.99	26.45
Silty clay	19.93	19.97	20.02	20.16	20.23	20.44	20.81	21.59	23.66	32.47
Light clay	18.50	18.54	18.60	18.69	18.83	19.05	19.45	20.28	22.48	31.60

Table 2.5 Average relative error in percent for all combinations of soil and vegetation-types.

	Crop./ Pasture	Crop. irrigated	Crop.-non- irrigated	Crop./ Grassland	Crop/ Woodland	Grassland	Shrubland	Shrubland/ Grassland	Savanna	Decid. b.-leaf
Sand	9.48	9.48	9.48	9.48	9.48	9.48	9.57	9.51	9.49	9.49
Loamy Sand	9.48	9.48	9.48	9.48	9.49	9.48	9.64	9.54	9.50	9.49
Sandy Loam	9.48	9.48	9.48	9.48	9.49	9.48	9.61	9.54	9.49	9.49
Silty Loam	9.49	9.49	9.49	9.49	9.50	9.49	9.74	9.60	9.52	9.51
Silt	9.49	9.49	9.49	9.49	9.50	9.49	9.74	9.59	9.52	9.51
Loam	9.49	9.49	9.49	9.49	9.49	9.49	9.67	9.56	9.51	9.50
S. C. Loam	9.50	9.50	9.50	9.50	9.51	9.50	9.92	9.68	9.55	9.53
Sil. C. Loam	9.60	9.60	9.60	9.60	9.71	9.60	11.1	10.38	9.87	9.79
Clay Loam	9.53	9.54	9.53	9.53	9.59	9.53	10.43	9.97	9.68	9.63
Sandy Clay	9.49	9.49	9.49	9.49	9.50	9.49	9.73	9.59	9.52	9.51
Silty Clay	9.64	9.65	9.65	9.64	9.78	9.64	11.42	10.61	9.99	9.88
Light Clay	9.72	9.73	9.73	9.72	9.91	9.72	11.88	10.94	10.17	10.04

Table 2.5 continued

	Decid.- needleleaf	Evergree n broadleaf	Evergreen needlleaf	Mixed Forest	Herb.- Wetland	Wooded Wetland	Herb.- Tundra	Wooded Tundra	Mixed Tundra	Tundra
Sand	9.50	9.49	9.49	9.49	9.48	9.49	9.55	9.51	9.55	9.60
Loamy Sand	9.51	9.50	9.50	9.50	9.49	9.50	9.60	9.54	9.60	9.69
Sandy Loam	9.51	9.50	9.50	9.50	9.49	9.49	9.58	9.53	9.58	9.66
Silty Loam	9.54	9.52	9.53	9.52	9.50	9.51	9.68	9.59	9.68	9.81
Silt	9.54	9.52	9.53	9.52	9.50	9.51	9.68	9.59	9.68	9.81
Loam	9.52	9.51	9.51	9.51	9.49	9.50	9.63	9.56	9.63	9.73
S. C. Loam	9.58	9.54	9.56	9.55	9.51	9.54	9.82	9.67	9.82	10.04
Sil.C. Loam	10.02	9.86	9.91	9.88	9.69	9.83	10.83	10.34	10.83	11.42
Clay Loam	9.76	9.67	9.70	9.68	9.58	9.65	10.25	9.95	10.25	10.64
Sandy Clay	9.54	9.52	9.53	9.52	9.50	9.51	9.68	9.59	9.68	9.81
Silty Clay	10.18	9.98	10.04	10.00	9.76	9.93	11.12	10.55	11.12	11.79
Light Clay	10.41	10.17	10.24	10.12	9.87	10.10	11.54	10.87	11.54	12.29

3. UNCERTAINTY OF PREDICTED GROUND HEAT FLUX DENSITY

The method described in the Chapter 2 in Section 3 is also applied to ground heat flux.

The simulation discussed in the following text is the same as described in the paper.

3.1 GROUND HEAT FLUX

In the OSULSM (CHEN and DUDHIA, 2001), the governing heat balance equation is determined by the simplified equation of diffusion (e.g. MAHRT and EK, 1984)

$$C(\eta) \frac{\partial T}{\partial t} = \frac{\partial}{\partial z} \left[\lambda(\eta) \frac{\partial T}{\partial z} \right] \quad (12)$$

Herein, C is soil volumetric heat capacity described as (CHEN and DUDHIA, 2001)

$$C = \eta C_w + (1 - \eta) C_s + (\eta_s - \eta) C_a \quad (13)$$

where, η is volumetric water content ($\text{m}^3 \text{m}^{-3}$), η_s ($\text{m}^3 \text{m}^{-3}$) is porosity, C_w , C_s and C_a ($\text{Jm}^{-3} \text{K}^{-1}$) are the volumetric heat capacity of water, soil and air, respectively.

Ground heat flux

$$H_s = \lambda(\mu) \frac{\partial T}{\partial z} \quad (14)$$

is a function of thermal conductivity, $\lambda(\eta)$ and soil vertical temperature gradient $\frac{\partial T}{\partial z}$.

Furthermore, the dependence of λ on volumetric water content, η , and soil pore size distribution index, b , is formulated in accord with McCUMBER (1980)

$$\lambda = \begin{cases} 420 \exp(-(2.7 + P_f)) & P_f \leq 5.1 \\ 0.1744 & P_f > 5.1 \end{cases} \quad (15)$$

where P_f is described as

$$P_f = -b \log_{10} \eta \quad \eta > 0 \quad (16)$$

Note that pore-size distribution index, b is an empirical soil parameter that is characteristic for each soil type.

Other LSMs using Eq. (15) or similar to parameterize thermal conductivity are the soil model by McCUMBER and PIELKE (1981), HTSVS (KRAMM et al., 1996; MÖLDERS et al., 2003). Examples of LSM's using Eqs. (13) and (14) are BATS (e.g., DICKINSON et al., 1993), SEWAB (e.g., MENGELKAMP et al., 1999) and CLASS (e.g., VERSEGHY, 1991; VERSEGHY et al., 1993).

3.2 ANALYSIS

In the parameterization of $\lambda(\eta)$, the only empirical parameter is b . Values of b for different soil types and their standard deviations are taken from COSBY (1984) and are presented in Table 3.1. Uncertainty in ground heat flux density is estimated for a typical range of meteorological and soil conditions. Relative volumetric water content, $\frac{\eta}{\eta_s}$, is varied from $0.01 \text{ m}^3 \text{ m}^{-3}$ to $1 \text{ m}^3 \text{ m}^{-3}$. The vertical temperature gradient varies from -50 K m^{-1} to 50 K m^{-1} .

3.3 RESULTS OF THEORETICAL STUDY AND NWP EXAMPLE

Typically, regardless of soil-type, ground heat flux increases as η approaches η_s and $\frac{\partial T}{\partial z}$ increases (Figure 3.1). Uncertainty shows similar behavior. The increase in uncertainty is the most rapid for small values of relative volumetric content and strong temperature gradients (deserts). This pattern is the most pronounced for sand and the variety of soils with a great percentage of sand. On the other hand, small variations in soil temperature and wetter soil conditions result in reduced uncertainty. For most soil types uncertainty reaches its maximum at relative volumetric water content, reaching 60% - 80% of saturation and a strong temperature gradient. For the temperature range examined here the greatest relative error is found for sandy clay loam (202%). The lowest one occurs for sandy clay (57%). Based on those high relative errors one has to conclude that a less uncertainty-burdened parameterization should be identified and implemented in the future.

In the NWP great uncertainty is strongly related to the dry and cloud free areas of the domain. As expected from the theoretical results clay loam and loam are the soil-types for which the greatest uncertainty in ground heat flux density is found. Soil-type averaged uncertainty displays a diurnal cycle (Figure 3.2). The average relative error in simulation of ground heat flux is 54%. The uncertainty values are on the order of 10Wm^{-2} and thus less than the typical errors in ground heat flux measurements.

REFERENCES

- CHEN, F., and J. DUDHIA, 2001: Coupling an advanced land surface hydrology model with the Penn State/NCAR MM5 modeling system. Part I: Model description and implementation. - *Mon. Wea. Rev.*, **129**, 569-585.
- COSBY, B.J., G.M. HORNBERGER, R.B. CLAPP, and T.R. GINN, 1984: A statistical exploration of the relationships of soil moisture characteristics to the physical properties of soils. - *Water Resour. Res.*, **20**, 682-690.
- DICKINSON, R.E., A. HENDERSON-SELLERS, and P.J. KENNEDY, 1993: Biosphere Atmosphere Transfer Scheme (BATS) version 1e as coupled to the NCAR Community Climate Model. NCAR Technical Note, NCAR/TN-378+STR
- KRAMM, G., N. BEIER, T. FOKEN, H. MÜLLER, P. SCHRÖDER, and W. SEILER, 1996: A SVAT scheme for NO, NO₂, and O₃ - model description. - *Meteorol. Atmos. Phys.*, **61**, 89-106.
- MAHRT, L. AND M. EK, 1984: The influence of atmospheric stability on potential evaporation.-*J. Clim. Appl. Meteorol.*, **23**, 222-234.
- MENGELKAMP, H.-T, K. WARRACH and E. RASCHKE, 1999: SEWAB – a parameterization of the Surface Energy and Water Balance for atmospheric and hydrologic models. – *Adv. Water Res.*, **23**, 165-175
- McCUMBER, M.C., 1980: A numerical simulation of the influence of heat and moisture fluxes upon mesoscale circulation.-. PhD Thesis, University of Virginia, USA, 255 pp.

- McCUMBER, M.C. and R.A. PIELKE, 1981: Simulation of the effects of surface fluxes of heat and moisture in a mesoscale numerical model - Part 1: Soil layer. - *J. Geophys. Res.*, **86**, 9929-9938.
- MÖLDERS, N., U. HAFERKORN, J. DÖRING, and G. KRAMM, 2003: Long-term numerical investigations on the water budget quantities predicted by the hydro-thermodynamic soil vegetation scheme (HTSVS) – Part I: Description of the model and impact of long-wave radiation, roots, snow, and soil frost. - *Meteorol. Atmos. Phys.*, **84**, 115-135.
- VERSEGHY, D.L., 1991: CLASS – A Canadian land surface scheme for GCMs, 1, soil model. - *Int. J. Climatol.*, **11**, 111-133.
- VERSEGHY, D.L., N.A. McFARLANE, and M. LAZARE, 1993: A Canadian Land Surface Scheme for GCMs: II. Vegetation model and coupled runs. - *Int. J. Climatol.*, **13**, 347-370.

FIGURES

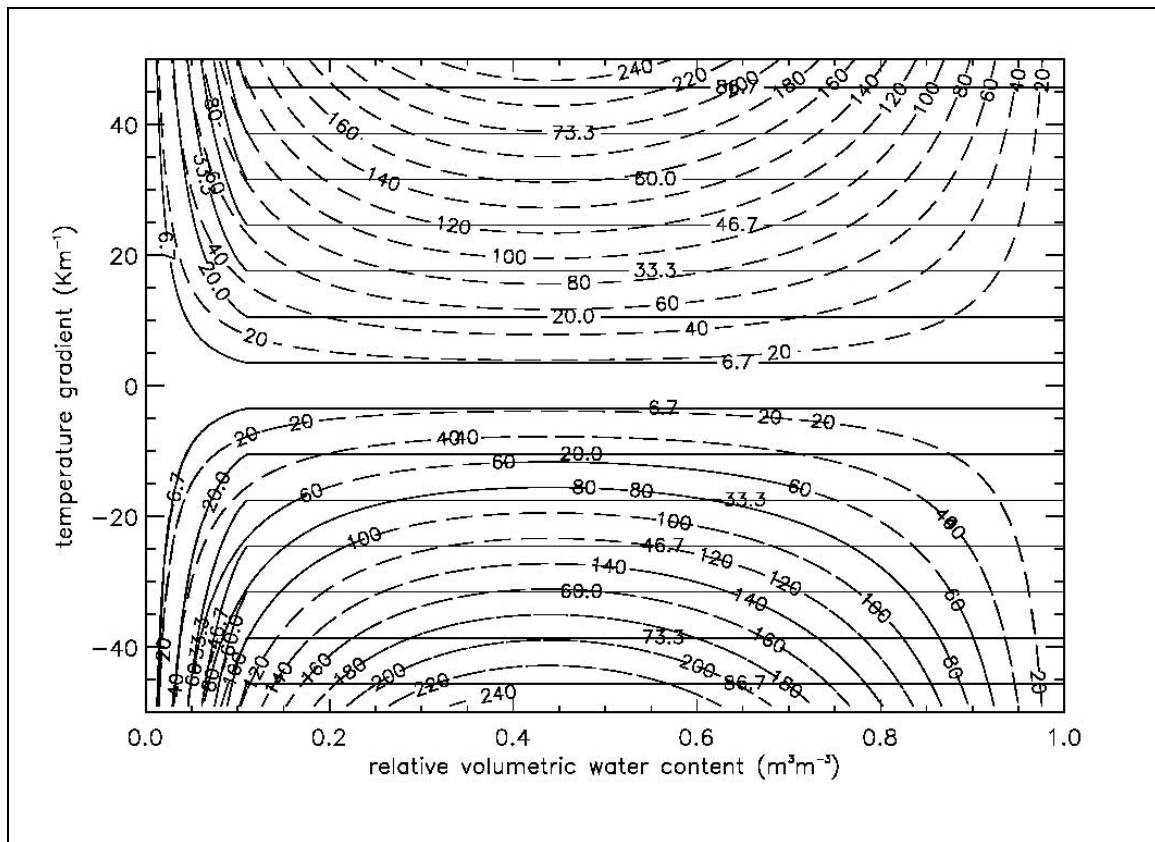


Figure 3.1 Ground heat flux density (Wm^{-2}) (solid lines) and its uncertainty (Wm^{-2}) (dashed lines) at various relative volumetric water content and soil temperature gradient values. Example shown is for sand. Note that the values of ground heat flux when relative volumetric water content exceeds $0.1 \text{ m}^3\text{m}^{-3}$ do not change for different temperature gradients. This behavior arises as a consequence of the limitations in the parameterization of thermal conductivity (see Eq. 15). Plots for all other soil types show the same qualitative behavior.

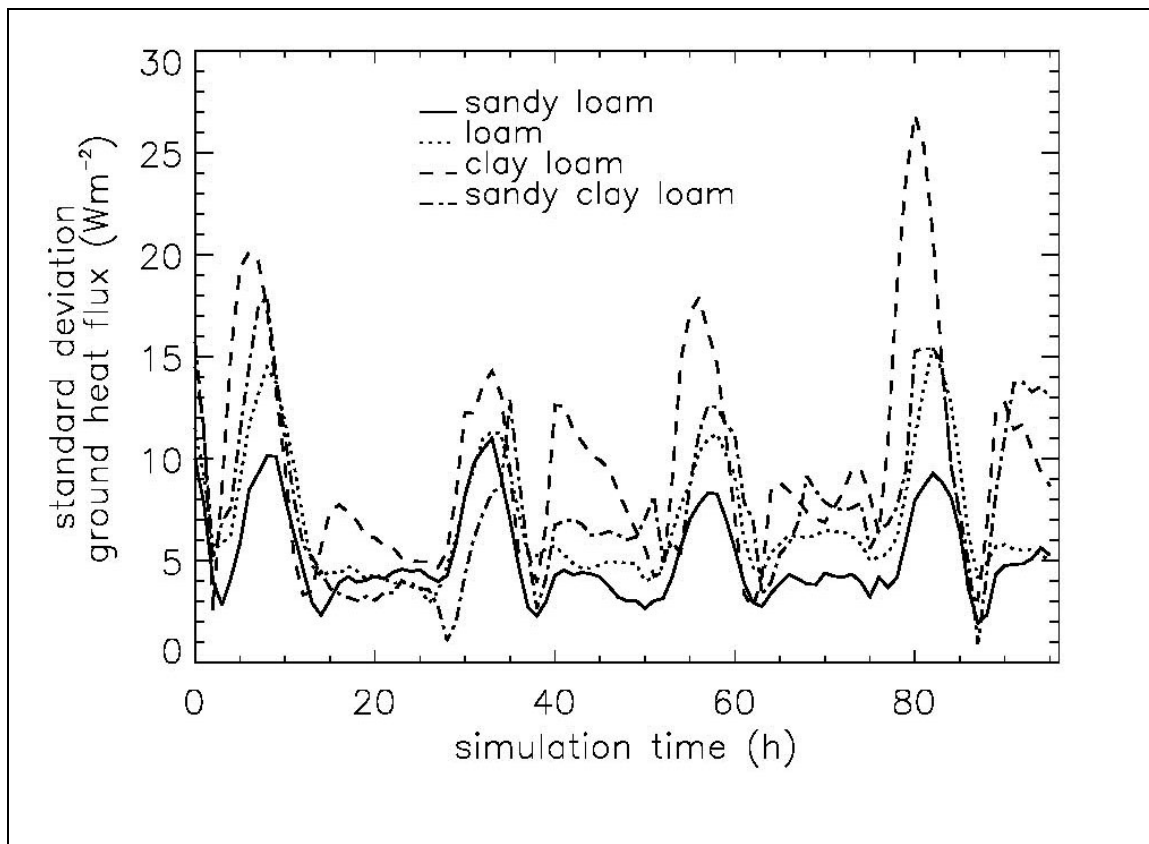


Figure 3.2 Temporal evolution of soil-type averaged uncertainty in ground heat flux density as obtained by the MM5 simulation. The shift in maxima is related to the location where the soil-types occur the most often. More western locations have their maxima later than the eastern region.

TABLES

Table 3.1 Pore size distribution index (-.-) and its standard deviations as obtained from COSBY et al. (1984).

Soil type	$b \pm \sigma_b$
Sand	2.79 ± 1.38
Loamy Sand	4.26 ± 1.95
Sandy loam	4.74 ± 1.4
Silty loam	5.33 ± 1.72
Silt	5.33 ± 1.72
Loam	5.25 ± 1.66
Sandy clay loam	6.66 ± 3.39
Silty clay loam	8.72 ± 4.33
Clay loam	8.17 ± 3.74
Sandy clay	10.73 ± 1.54
Silty clay	10.39 ± 4.27
Light clay	11.55 ± 3.93

4. CONCLUSIONS

Uncertainty of evapotranspiration and ground heat flux density caused by empirical parameters is assessed by the Gaussian error propagation principles for various ranges of soil and atmospheric forcing conditions. In addition, the uncertainty behavior of these quantities is demonstrated for a numerical weather prediction example.

The study shows that the predictability of ground heat flux as parameterized in OSULSM and many other LSMs is strongly impacted by the uncertainty in thermal conductivity. The pore-size distribution index is the only empirical soil parameter used in the parameterization of thermal conductivity. To achieve less uncertain values of calculated thermal conductivity pore-size distribution index must be determined with higher accuracy than currently available (Table 3.1). As seen from the numerical weather prediction example and the theoretical analysis, prediction of ground heat fluxes over drier and warm regions is particularly burdened with uncertainty and limits predictability especially in deserts, during droughts and long dry periods in summer.

The greatest average relative errors are found for sandy clay loam (202%) and sandy (192%) implying that pore-size distribution index for these respective soils should be determined more precisely. A better parameterization of thermal conductivity can also improve the overall predictability of ground heat flux (see MÖLDERS, 2005).

In the analysis of evapotranspiration maximal canopy storage and shielding factor are identified as the most critical parameters in E_t and E_{can} , especially in scarcely vegetated areas, for which these parameters should be determined with higher accuracy.

Over well vegetated regions uncertainty in evapotranspiration is dominated by the uncertainty in E_{dir} .

In the future, uncertainty in predicted state variables like soil moisture and temperature, snow temperature and water content, skin temperature, snow surface temperature and canopy water have to be determined to assess the uncertainty of the parameters investigated here more thoroughly and to examine the impact of empirical parameters that are used in other parts of the OSULSM.